

RESEARCH PAPER



# Design, synthesis, and biological evaluation of 5-((4-(pyridin-3-yl)pyrimidin-2-yl)amino)-1*H*-Indole-2-Carbohydrazide derivatives: the methuosis inducer **12A** as a Novel and selective anticancer agent

Jun Wu<sup>a\*</sup>, Hongyu Hu<sup>b\*</sup>, Mingtao Ao<sup>a\*</sup>, Zhenzhen Cui<sup>a</sup>, Xiaoping Zhou<sup>a</sup>, Jingbo Qin<sup>a</sup>, Yafei Guo<sup>a</sup>, Jingwei Chen<sup>a</sup>, Yuhua Xue<sup>a</sup> and Meijuan Fang<sup>a</sup>

<sup>a</sup>School of Pharmaceutical Sciences and School of Public Health, Xiamen University, Xiamen 361102, China; <sup>b</sup>Xingzhi College, Zhejiang Normal University, Lanxi, China

## ABSTRACT

This study describes the synthesis and vacuole-inducing activity of 5-((4-(pyridin-3-yl)pyrimidin-2-yl)amino)-1*H*-indole-2-carbohydrazide derivatives, including five potent derivatives **12c**, **12g**, **12i**, **12n**, and **12A** that exhibit excellent vacuole-inducing activity. Remarkably, **12A** effectively induces methuosis in tested cancer cells but not human normal cells. In addition, **12A** exhibits high pan-cytotoxicity against different cancer cell lines but is hardly toxic to normal cells. It is found that the **12A**-induced vacuoles are derived from macropinosomes but not autophagosomes. The **12A**-induced cytoplasmic vacuoles may originate from the endoplasmic reticulum (ER) and be accompanied by ER stress. The MAPK/JNK signalling pathway is involved in the **12A**-induced methuotic cell death. Moreover, **12A** exhibits significant inhibition of tumour growth in the MDA-MB-231 xenograft mouse model. The excellent potency and selectivity of **12A** prompt us to select it as a good lead compound for further development of methuosis inducers and investigation of the molecular and cellular mechanisms underlying methuosis.

## GRAPHICAL ABSTRACT HIGHLIGHTS

- Novel methuosis-inducing anticancer agents are designed and synthesised.
- Vacuole inducers **12i** and **12A** display high anticancer activity and little-toxic to normal cells.
- Compound **12A** is a selective methuosis inducer involving the activation of MAPK/JNK signalling pathway.
- Compound **12A** effectively inhibits tumour growth in the MDA-MB-231 xenografted mouse model.

## ARTICLE HISTORY

Received 1 February 2021  
Revised 31 May 2021  
Accepted 3 June 2021

## KEYWORDS

1*H*-indole-2-carbohydrazide derivatives; Methuosis; Anticancer agent; MDA-MB-231 cells


## 1. Introduction

To date, numerous anticancer agents have been developed and some have been widely used in clinical therapy, but cancer remains one of the leading causes of death worldwide<sup>1–3</sup>. In general, the existing anticancer drug treatments are mainly based on inducing programmed cell death (PCD). However, tumour suppressor genes controlling PCD in cancer cells are often mutated, which can render cancer cells relatively insensitive to apoptosis and eventually confer them a multidrug resistance phenotype to these conventional chemotherapeutic drugs typically targeting apoptosis. Therefore, small molecules killing cancer cells *via* non-apoptotic cell death mechanisms are considered as a promising therapeutic strategy for those cancers that are insensitive to apoptosis-inducing drugs. It has been demonstrated that methuosis plays a key role in various physiological processes, including neural development and the death of retinal pigment epithelial cells<sup>1,2</sup>. In addition, methuosis has been reported as an important non-apoptotic cell death pathway<sup>3–5</sup>, and thus,

methuosis inducers have emerged as a novel class of potential therapeutic agents for cancer treatment, especially the treatment of therapy-resistant cancers. Several types of methuosis inducers with different scaffolds are shown in Figure 1<sup>6–12</sup>. Among them, the (*E*)-3-(1*H*-indol-3-yl)-1-(pyridin-4-yl)prop-2-en-1-one (IPP) derivatives have emerged as a promising type of methuosis inducer<sup>7,11</sup>. Several IPP molecules, including 3-(2-methyl)-IPP (MIPP) and 3-(5-methoxy-2-methyl)-IPP (MOMIPP), have been developed as potent methuosis inducers<sup>13</sup>. MIPP and MOMIPP could induce vacuolization and lead to non-apoptotic cell death in various cancer cell lines, including non-resistant (*e.g.* LN229, MCF7, U251, MDA-MB-468, A549) and resistant (adriamycin-resistant MCF7 and temozolomide-resistant U251) cells. Initially, it was found that the indolyl and pyridinyl moieties of IPP molecules exhibited a high degree of structural specificity for the induction of methuosis. Since then, extensive research has been conducted on the analysis of the quantitative structure-activity relationship (QSAR) of IPP

**CONTACT** Meijuan Fang  [48338024@qq.com](mailto:48338024@qq.com); Yuhua Xue  [xueyuhua@xmu.edu.cn](mailto:xueyuhua@xmu.edu.cn); Jingwei Chen  [jwchen@xmu.edu.cn](mailto:jwchen@xmu.edu.cn)  School of Pharmaceutical Sciences and School of Pharmaceutical Sciences, Xiamen University, South Xiang-An Road, Xiamen 361102, China

\*These authors contributed equally to this work.

 Supplemental data for this article can be accessed [here](#).

© 2021 The Author(s). Published by Informa UK Limited, trading as Taylor & Francis Group.

This is an Open Access article distributed under the terms of the Creative Commons Attribution-NonCommercial License (<http://creativecommons.org/licenses/by-nc/4.0/>), which permits unrestricted non-commercial use, distribution, and reproduction in any medium, provided the original work is properly cited.

derivatives, focussing on the substitutions at the 6- and 2-indolyl position<sup>8,13</sup>. Notably, in 2018, one azaindole derivative (compound 13) was identified as a highly selective and potent methuosis inducer, which exhibited a remarkable tumour-suppressive effect in the MDA-MB-231 xenograft mouse model<sup>10</sup>. In recent years, more and more studies have shown that the therapeutic use of methuosis-inducing agents can be considered as a potential anti-cancer strategy<sup>14</sup>.

Many compounds containing the 4-(pyridin-3-yl)pyrimidine moiety show good anticancer activity<sup>15–19</sup>. For example, imatinib, a representative anticancer agent with the 4-(pyridin-3-yl)pyrimidine moiety, is the first thymidine kinase inhibitor to be introduced into the market (in 2002 under the name “Glivec”) and is still being used against certain types of cancer, such as chronic and acute leukaemia. In addition, we previously found that the 1*H*-indole-2-carbohydrazide derivative **3 b** was a good anticancer agent<sup>20</sup>. Thus, we developed an idea to find new methuotic anticancer agents that involved combining key pharmacophores of imatinib, MOMIPP, and **3 b** to produce three classes of target compounds (series A, B, and C) (Figure 2). Firstly, we synthesised the three classes of target compounds (series A, B, and C) and then evaluated them for their vacuolization effect and antitumor activity. Notably, several synthesised compounds (e.g. **12 g**, **12 i**, **12 n**, **12 A**) were identified as potent vacuolization-inducing agents with excellent antitumor activity and low toxicity to normal cells *in vitro*. Furthermore, *in vivo* antitumor efficacy of compound **12 A**

was evaluated in an MDA-MB-231 xenograft mouse model, and its mechanisms of antitumor activity were probed, by assessing its methuosis, autophagy, and apoptosis inducing effects. In summary, **12 A**, which showed potent cytotoxic activity against a broad panel of cancer cell lines but low toxicity to human normal cells, was selected as a promising lead compound for further development as a potent methuosis inducer for use in cancer therapy.

## 2. Results and discussion

### 2.1. Chemistry

The synthetic routes of target compounds are outlined in Scheme 1 and Scheme 2. First, we synthesised (*E*)-*N'*-methylene-4-(3-(4-methyl-3-(4-(pyridin-3-yl)pyrimidin-2-yl)amino)phenyl)ur-ido)-1*H*-indole-2-carbohydrazide derivatives (**8a–8f**). As shown in Scheme 1, the general chemistry for the synthesis of **8a–8f** was adapted from previously reported methods<sup>20–22</sup>. Briefly, 1-(4-nitrophenyl)hydrazine (**1**) was refluxed with ethyl 2-oxopropanoate in ethanol to give compound **2**, which then underwent ring closure with polyphosphoric acid to form intermediate **3**. Catalytic hydrogenation of the nitro group of compound **3** with palladium on carbon (Pd/C) afforded **4**, which was followed by reaction with triphosgene in tetrahydrofuran (THF) to produce compound **5**. Subsequently, the intermediate **5** reacted with 6-methyl-*N'*-(4-(pyridin-3-yl)pyrimidin-2-yl)benzene-1,3-diamine to give ethyl 4-(3-(4-

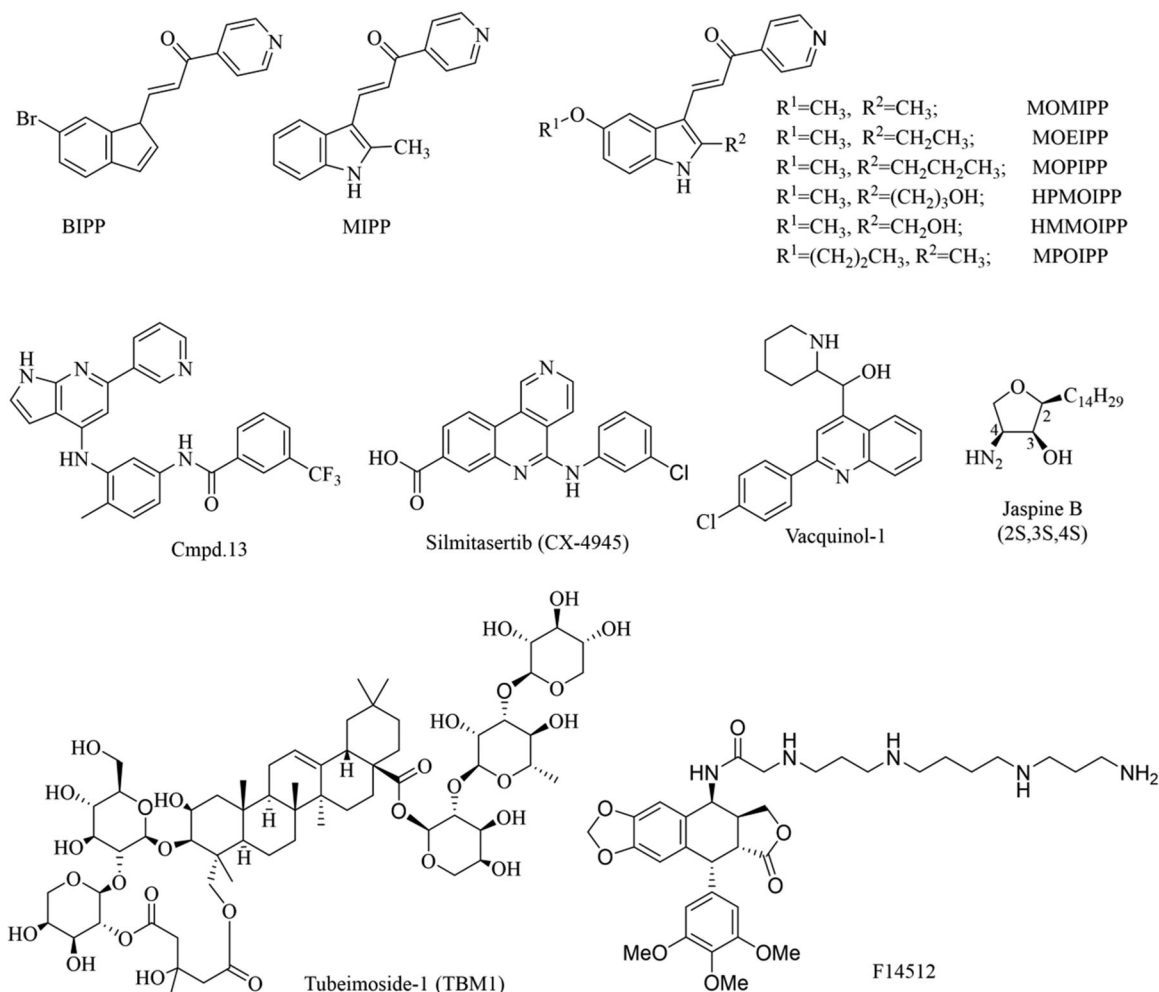


Figure 1. The chemical structures of several representative methuosis inducers.

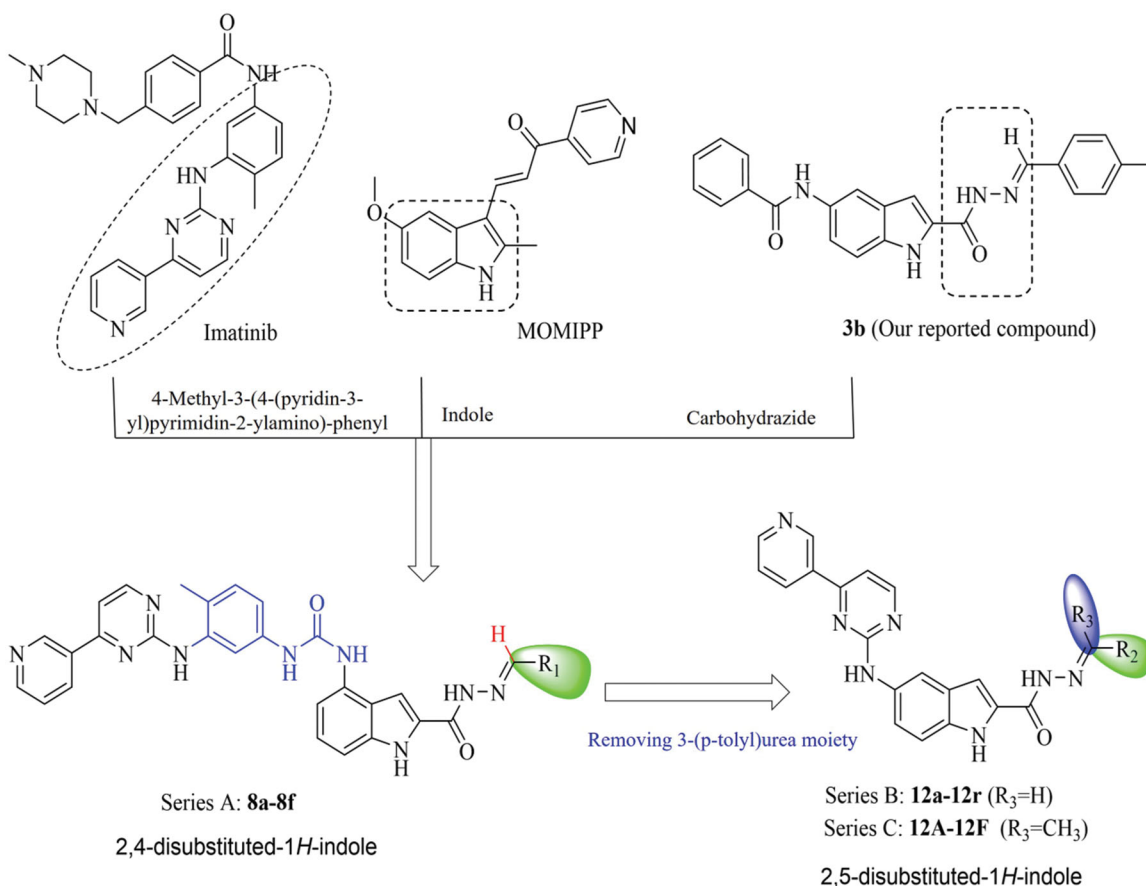


Figure 2. Design and modification strategies of target compounds.

methyl-3-((4-(pyridin-3-yl)pyrimidin-2-yl)amino)phenyl)ureido)-1H-indole-2-carboxylate (**6**). Compound **6** was treated with hydrazine hydrate in refluxing ethanol to afford **7**, which was subjected to reactions with various aldehydes to produce the corresponding compounds **8a-8f**.

The synthesis of compounds **12a-12r** (Series B) and compounds **12A-12F** (Series C) is shown in Scheme 2. The intermediate **10** was obtained from compound **4**<sup>23</sup>. Compound **4** was refluxed with cyanamide in ethanol with concentrated HCl for 24 h, then treated with NH<sub>4</sub>NO<sub>3</sub> to produce ethyl 5-guanidino-1H-indole-2-carboxylate (**9**). The intermediate **9** was reacted with 3-(dimethylamino)-1-(3-pyridinyl)prop-2-en-1-one in the presence of NaOH under reflux condition in ethanol for 72 h to give **10** which was then converted to **11** upon reaction with hydrazine hydrate in refluxing ethanol. Ultimately, compound **11** was separately reacted with different aldehydes or methyl ketones in refluxing ethanol to produce the corresponding target compounds of series B (**12a-12r**) and series C (**12A-12F**), respectively.

## 2.2. Biological activity

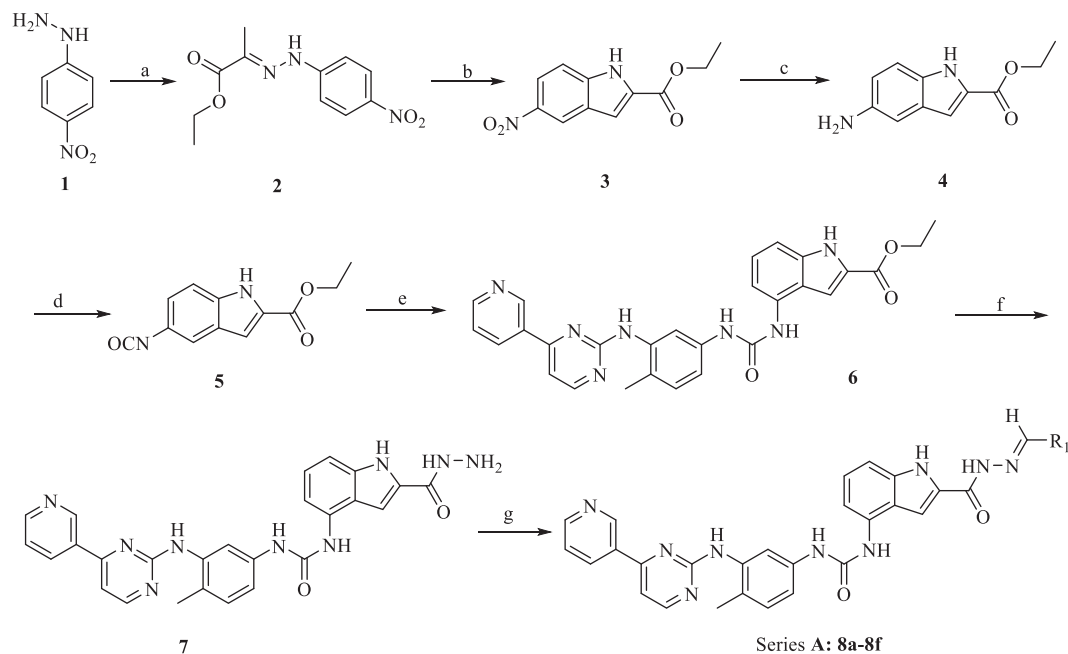
### 2.2.1. Identification of effective vacuolization inducers with anti-cancer activity and analysis of the structure-activity relationships

To identify effective methuosis inducing agents for use as anti-cancer drugs, both the vacuolization effect and antiproliferative activities of target compounds **8a-8f**, **12a-12r**, and **12A-12F** were evaluated in HeLa cells. HeLa cells were treated with different compounds with a low concentration (1.0 μM) for 8 h to evaluate the vacuolization-inducing effect of target compounds.

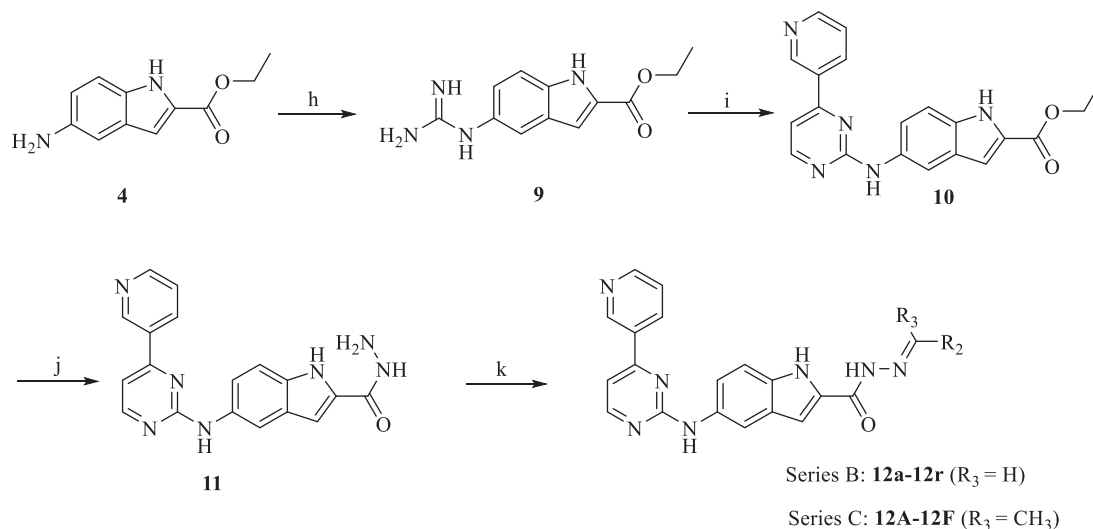
Similarly, the antiproliferative effect of all synthesised compounds at 1.0 and 20.0 μM was evaluated in HeLa cells after 48 h treatment. MOMIPP was used as a positive control. The vacuolization effect and cell growth inhibition results for all target compounds are summarised in Tables 1-3.

First, we investigated the functionality of the key pharmacophores from imatinib at the 4-position of the indole ring. Compounds **8a-8f** (Table 1) had no growth inhibitory (GI) activity against HeLa cells at the tested concentration range and also did not induce vacuolization at 1.0 μM. However, when the 1-(p-tolyl)urea moiety was deleted and the residue (4-(pyridin-3-yl)pyrimidin-2-yl)amino was transferred to the 5-position of the indole ring, there was a significant increase in the vacuolization-inducing effect. For example, treatment with **8a**, **8b**, and **8c** had no vacuolization-inducing effect (Table 1), whereas compounds **12c**, **12d**, and **12p** showed a vacuolization-inducing effect to various degrees at 1.0 μM (Table 2), with a vacuolization ratio of 89 ± 0.55%, 74 ± 0.56%, and 73 ± 1.56%, respectively. These data suggested that the functional group should be substituted at the 5-position of the indole ring and the 1-(p-tolyl)urea moiety might be unhelpful for vacuole-inducing effect.

Next, we turned our attention to Series B compounds of the acyl hydrazones (R<sub>3</sub>=H). More than half of the Series B compounds exhibited a vacuolization-inducing effect on HeLa cells at 1.0 μM (Table 2). Among the alkyl-substituted compounds, **12c** (*n*-butyl) induced extensive vacuolization, while **12a** (ethyl) and **12b** (propyl) completely lost the ability to induce vacuolization. These results suggested that the chain space volume of *n*-alkyl group at R<sub>2</sub> plays an important role in determining the vacuolization-inducing effect. Compound **12c** had an excellent vacuolization-inducing



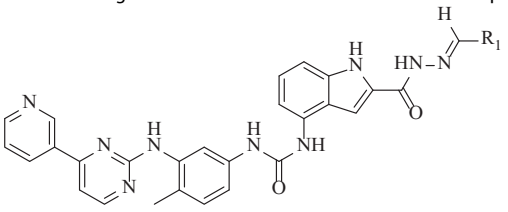
**Scheme 1.** Synthetic route of target compounds **8a–8f** (Series A). Reagents and conditions: (a) ethyl 2-oxopropanoate, EtOH, reflux, for 2 h; (b) polyphosphoric acid, at 100 °C, for 1 h; (c) 10% Pd/C, H<sub>2</sub>; (d) triphosgene, THF, triethylamine at 0 °C, for 4 h; (e) 6-methyl-*N*<sup>1</sup>-(4-(pyridin-3-yl)pyrimidin-2-yl)-benzene-1,3-diamine, toluene, at 60 °C, 4 h; (f) hydrazine hydrate, EtOH, reflux, for 6 h; (g) RCHO, EtOH, reflux, for 8 h.

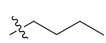
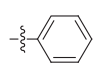
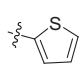
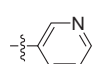
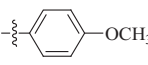
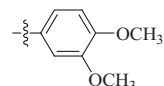


**Scheme 2.** Synthetic route of target compounds **12a–12r** (Series B) and **12A–12F** (Series C). Reagents and conditions: (h) ① H<sub>2</sub>CN, concentrated HCl, EtOH, reflux, for 24 h, ② NH<sub>4</sub>NO<sub>3</sub> (aq); (i) 3-(dimethylamino)-1-(3-pyridinyl)prop-2-en-1-one, NaOH, EtOH, reflux, for 72 h; (j) hydrazine hydrate, EtOH, reflux, for 6 h; (k) RCHO/RCOCH<sub>3</sub>, EtOH, reflux, for 8 h.

effect, but a weak antiproliferative effect. Accordingly, we replaced the *n*-butyl group with a phenyl group to afford compound **12d**, which induced moderate vacuolization and showed a modest antiproliferative effect. When the R<sub>2</sub> moiety was the ortho-substituted phenyl group, compounds with 2-chlorophenyl (**12e**), 2-hydroxyphenyl (**12f**), and 2-methoxyphenyl (**12g**) substitutions, showed different vacuolization-inducing effects with vacuolization rate values at 1.0 μM of 41 ± 0.91%, 3 ± 0.81%, and 98 ± 0.45%, respectively. These results indicated that the introduction of a strong electron-donating group (–OCH<sub>3</sub>) on the 2-position of the benzene ring was beneficial for the induction of vacuolization, which might be mainly due to the formation of electronic interactions between the R<sub>2</sub> group and the target(s). However, para-substituted phenyl acyl hydrazones, such as **12i** (4-methylphenyl)

exhibited potent vacuolization-inducing effect with vacuolization rate values at 1.0 μM of 94 ± 3.21%, while **12h** (4-methoxyphenyl) showed almost no vacuolization-inducing effect. This result further confirmed that the size of R<sub>2</sub> is crucial for maintaining the inhibitory effect. In compounds **12k–12o** which contain di- or tri-substituted phenyl ring (R<sub>2</sub>), the substituted positions of the substituents showed an important relationship with the vacuolization-inducing effect. Compounds **12k** (3-hydroxy-4-methoxyphenyl) and **12l** (2,3-dimethoxyphenyl) showed a similar level of effect. The 3,5-dimethoxy derivative, compound **12n**, showed a dramatically increased vacuolization effect at 1.0 μM and exhibited potent inhibition of cell growth at 20.0 μM. However, treatment with compound **12m** (2,4-dimethoxyphenyl) had a weak vacuolization-inducing effect on HeLa cells. Compound **12o** with the

**Table 1.** Summary of the vacuolization effect and cell growth inhibition evaluation results for compounds **8a–8f** (Series A) in HeLa Cells.


ID	R <sub>1</sub>	Vacuolization ratio (%) (1 μM)	Cell growth inhibition rate (%)		ID	R <sub>1</sub>	Vacuolization ratio (%) (1 μM)	Cell growth inhibition rate (%)	
			1 μM	20 μM				1 μM	20 μM
<b>8a</b>		<1±0.15	-3±0.25	-1±0.62	<b>8b</b>		<1±0.87	-5±0.34	14±0.52
<b>8c</b>		<1±0.23	9±0.13	13±0.33	<b>8d</b>		<1±0.14	0±0.23	2±0.32
<b>8e</b>		<1±0.21	-1±0.25	1±0.35	<b>8f</b>		<1±0.18	1±0.43	3±0.51
<b>MOMIPP</b>		99±0.5	3±0.34	70±0.45	<b>Imatinib</b>		<1±0.12	11±0.33	21±0.42

3,4,5-trimethoxyphenyl substitution also lost the ability to induce vacuolization at 1.0 μM. Taken together, the shape of the R<sub>2</sub> group plays a crucial role in determining the vacuolization-inducing effect. In addition, we investigated the impact of other aromatic groups at R<sub>2</sub> on the vacuolization-inducing effect. A comparison of the effects of compounds **12p** and **12q** with **12d**, as shown in [Table 2](#), revealed that the five-membered aromatic heterocycle substitutions, such as thiophen-2-yl and furan-2-yl groups, had a similar effect as a phenyl group, but the replacement of the phenyl group with a 4-methoxynaphthalen-1-yl moiety resulted in the complete loss of the effect. The results also indicated that the introduction of the electron-rich aromatic ring has a beneficial effect on vacuolization and the size and shape of the R<sub>2</sub> group play a key role in determining the vacuolization-inducing effect.

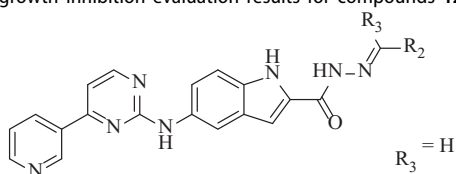
To further investigate the influence of the acyl hydrazone substituents on the biological effect of the pharmacophore, we replaced the two hydrogens of the acyl hydrazone methylene with methyl and (un)substituted phenyl groups, obtaining compounds **12A–12F**. The vacuolization effect and cell growth inhibition of compounds **12A–12F** in HeLa cells are summarised in [Table 3](#). Surprisingly, **12A** (R<sub>2</sub>=phenyl, R<sub>3</sub>=CH<sub>3</sub>) showed a significantly stronger effect than **12d** (R<sub>2</sub>=phenyl, R<sub>3</sub>=H) in both the growth inhibition and vacuolization assays, but **12D** (R<sub>2</sub>=4-methylphenyl, R<sub>3</sub>=CH<sub>3</sub>) dramatically decreased vacuolization and the inhibitory effect on cell growth compared with **12i** (R<sub>2</sub>=4-methylphenyl, R<sub>3</sub>=H). These results indicated that the global shape and size of the substituents R<sub>2</sub> and R<sub>3</sub> played an important role in determining the vacuolization-inducing effect, which might be determined by the joint formation of the key interactions of the two substituents of methylene with their targets(s). In addition, we found that the replacement of the phenyl group with 4-chlorophenyl (**12B**) and 4-nitrobenzene (**12C**) moieties also significantly reduced the vacuolization-inducing effect at 1.0 μM. Additionally,

when the R<sub>3</sub> moiety was the di-substituted phenyl, compounds with 2-hydroxy-5-bromophenyl (**12E**) and 2-hydroxy-5-methoxyphenyl (**12F**) substitutions completely lost the ability to induce vacuolization, but **12E** caused a large reduction in the cell growth rate at the concentration of 20 μM. These results further demonstrated that the global shape and size of the substituents R<sub>2</sub> and R<sub>3</sub> were crucial for maintaining the vacuolization-inducing effect. Finally, the preliminary structure and activity relationships are summarised in an illustration in [Figure S1](#) in the Supporting Information.

Overall, five compounds (**12c**, **12g**, **12i**, **12n**, and **12A**) at 1.0 μM showed similar vacuolization-inducing effects as the reference compound MOMIPP, thus these five compounds were selected for further evaluation of their antiproliferative activities against human cancer and normal cells using the MTT assay based on the degradation of 3-(4, 5-dimethylthiazol-2-yl)–2,5-diphenyltetrazolium bromide (MTT). As shown in [Table 4](#), compound **12c** did effectively induce vacuolization at 1.0 μM but did not affect the cell growth rate of cancer and normal cells, with half-maximal inhibitory concentration (IC<sub>50</sub>) values above 50 μM. However, the other four compounds showed both significant vacuolization-inducing effect and a broad spectrum of cytotoxicity against cancer cells with IC<sub>50</sub> values in the low micromolar range, but low cytotoxicity to normal cells. This finding implies that one aryl substitution on acyl hydrazone methylene plays a key role in the anti-tumor activity.

### 2.2.2. Compound **12A** effectively induces cytoplasmic vacuolization in cancer cells

After considering both the vacuolization and anticancer effects ([Table 4](#)), we selected **12A** for further biological assays. First, the ability of **12A** to induce vacuolization in different types of cells

**Table 2.** Summary of the vacuolization effect and cell growth inhibition evaluation results for compounds **12a–12r** (Series B) in HeLa Cells.

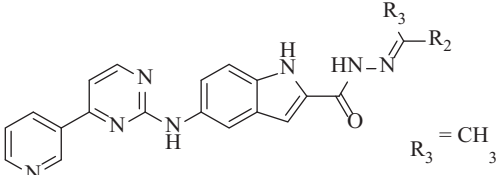
ID	R <sub>2</sub>	Vacuolization ratio(%) (1 $\mu$ M)	Cell growth inhibition rate (%)		ID	R <sub>2</sub>	Vacuolization ratio(%) (1 $\mu$ M)	Cell growth inhibition rate (%)	
			1 $\mu$ M	20 $\mu$ M				1 $\mu$ M	20 $\mu$ M
12a		<1 $\pm$ 1.1	1 $\pm$ 0.56	-1 $\pm$ 0.36	12b		<1 $\pm$ 0.67	5 $\pm$ 0.46	5 $\pm$ 0.66
12c		89 $\pm$ 0.55	10 $\pm$ 0.78	25 $\pm$ 0.89	12d		74 $\pm$ 0.56	19 $\pm$ 0.31	75 $\pm$ 0.25
12e		41 $\pm$ 0.91	23 $\pm$ 0.67	69 $\pm$ 0.57	12f		3 $\pm$ 0.81	65 $\pm$ 0.21	94 $\pm$ 0.98
12g		98 $\pm$ 0.45	18 $\pm$ 0.71	67 $\pm$ 0.62	12h		<1 $\pm$ 0.68	13 $\pm$ 0.34	15 $\pm$ 0.54
12i		94 $\pm$ 3.21	15 $\pm$ 0.76	76 $\pm$ 0.36	12j		5 $\pm$ 0.39	11 $\pm$ 0.99	44 $\pm$ 0.76
12k		60 $\pm$ 1.30	9 $\pm$ 0.45	15 $\pm$ 0.21	12l		50 $\pm$ 0.07	1 $\pm$ 0.34	6 $\pm$ 0.51
12m		10 $\pm$ 1.20	4 $\pm$ 0.52	15 $\pm$ 0.15	12n		92 $\pm$ 2.34	12 $\pm$ 0.23	72 $\pm$ 0.34
12o		15 $\pm$ 0.67	2 $\pm$ 0.56	70 $\pm$ 0.43	12p		73 $\pm$ 1.56	6 $\pm$ 0.62	12 $\pm$ 0.51
12q		55 $\pm$ 1.02	8 $\pm$ 0.19	86 $\pm$ 0.11	12r		4 $\pm$ 0.23	3 $\pm$ 0.21	-1 $\pm$ 0.34
MOMIPP		99 $\pm$ 0.5	3 $\pm$ 0.34	70 $\pm$ 0.45	Imatinib		<1 $\pm$ 0.12	11 $\pm$ 0.33	21 $\pm$ 0.42

was evaluated and the morphological changes were examined under a microscope. As shown in [Figure 3\(A\)](#), the number and the size of vacuoles increased markedly in **12A**-treated HeLa cells with increasing treatment time from 1 to 24 h. After treatment with 1  $\mu$ M **12A** for 1 h, small vesicles appeared in HeLa cells. The vesicles accumulated, fused, and formed larger vacuoles after treatment with 1  $\mu$ M **12A** for 16 h, becoming larger and more numerous after treatment for 24 h. Therefore, compound **12A** induced vacuolization in a time-dependent manner. Similarly, we also evaluated the effect of the treatment with **12A** at different concentrations on vacuolization in HeLa cells. As shown in [Figure 3\(B\)](#), vacuoles formation could be observed after treatment with 0.1  $\mu$ M **12A**. Vacuoles accumulated in HeLa cells after treatment

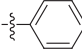
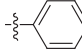
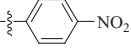
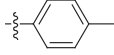
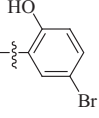
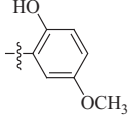
with **12A** at concentrations ranging from 0.1 to 2  $\mu$ M, implying that **12A** dose-dependently induced vacuole formation in HeLa cells. These results suggest that **12A** is an effective vacuolization inducer in HeLa cells, which can induce vacuole formation in a time- and dose-dependent manner. We also found that compound **12A** effectively induced vacuole formation in HeLa cells with a half-maximal effective concentration ( $EC_{50}$ ) value of  $0.26 \pm 0.02 \mu$ M, which was comparable to MOMIPP ( $EC_{50} = 0.18 \pm 0.05 \mu$ M). Then, to verify whether the **12A**-induced vacuolization also occurs in other cell lines, seven other different cancer cell lines (MDA-MB-231, HepG2, MCF-7, NT2, A549, A875, and A375) and three human normal cell lines (HaCat, MCF-10A, and LO2 cells) were evaluated after treatment with 1  $\mu$ M **12A** for 8 h. As shown in [Figure 3\(C\)](#),



**Table 3.** Summary of the vacuolization effect and cell growth inhibition evaluation results for compounds **12A–12F** (Series C) in HeLa Cells.



$R_3 = \text{CH}_3$

ID	R <sub>3</sub>	Vacuolization ratio (%) (1 μM)	Cell growth inhibition rate (%)		ID	R <sub>3</sub>	Vacuolization ratio (%) (1 μM)	Cell growth inhibition rate (%)	
			1 μM	20 μM				1 μM	20 μM
<b>12A</b>		96±1.02	16±0.51	82±0.07	<b>12B</b>		13±1.21	7±0.12	36±0.41
<b>12C</b>		40±1.12	4±0.35	6±0.32	<b>12D</b>		52±1.12	9±0.35	44±0.67
<b>12E</b>		<1±0.55	11±0.32	67±1.11	<b>12F</b>		1±0.73	9±0.91	1±0.52
<b>MOMIPP</b>		99±0.50	3±0.34	70±0.45	<b>Imatinib</b>		<1±0.12	11±0.33	21±0.42

**Table 4.** *In vitro* antiproliferative effects of selected compounds against cancer and normal cells

ID	Cancer cells (IC <sub>50</sub> , μM)				Normal cells (IC <sub>50</sub> , μM)	
	HepG <sub>2</sub>	HeLa	MDA-MB-231	MCF-7	MCF-10A	LO2
<b>12c</b>	>20	>20	>20	>20	>50	>50
<b>12g</b>	10.86 ± 0.20	9.75 ± 0.21	8.88 ± 0.41	3.36 ± 0.17	>50	>50
<b>12i</b>	8.25 ± 0.15	6.43 ± 0.18	3.81 ± 0.08	2.70 ± 0.13	>50	>50
<b>12n</b>	7.66 ± 0.24	7.46 ± 0.07	13.57 ± 0.06	2.84 ± 0.08	>50	>50
<b>12A</b>	5.63 ± 0.20	3.78 ± 0.15	4.51 ± 0.33	2.79 ± 0.15	185.7 ± 0.51	50.19 ± 0.35
<b>Imatinib</b>	28.08 ± 0.25	37.30 ± 0.22	28.19 ± 0.24	40.08 ± 0.35	39.37 ± 0.42	87.67 ± 0.31
<b>MOMIPP</b>	3.6 ± 0.045	5.2 ± 0.05	4.98 ± 0.11	4.5 ± 0.18	>50	>50

Cells were treated with indicated compounds for 48 h. Data are means ± SD of triplicate experiments.

**12A** induced vacuolization, to different extents, in the seven tested cancer cell lines, but not in the three normal cell lines. These data indicate that **12A** is an effective vacuolization inducer in cancer cells, but has almost no effect on normal human cells. Therefore, **12A** is a potent and selective vacuolization-inducer, which is consistent with the cell cytotoxicity analysis.

### 2.2.3. Compound **12A** induces the caspase-independent formation of macropinosome-derived cytoplasmic vacuoles

Since compound **12A** effectively inhibited cancer cell proliferation, it would be interesting to know whether **12A** induces PCD, such as cell apoptosis and cell cycle arrest. We found that the **12A**-induced vacuolization was not inhibited by Z-VAD-FMK (a pan-caspase inhibitor) in HeLa cells (Figure 4(A)). In addition, it was found that the cleaved PARP was hardly detected after treatment with

**12A** at low concentrations (<5 μM) (Supporting Information Figure S2). Consistently, only slight apoptosis was detected after the treatment with **12A** at concentrations below 5 μM (Supporting Information Figure S2). These findings indicate that the **12A**-induced vacuolization and cell growth inhibition might not be PARP cleavage-dependent. Additionally, very slight effects of **12A** on the cell cycle were observed in MDA-MB-231 cells (Supporting Information Figure S3). These data suggest that cell cycle arrest is not significantly involved in the inhibition of cancer cell proliferation by treatment with **12A**.

However, considering that in autophagic cells there are some autophagosome-like vacuoles, which sequester damaged cytoplasmic proteins and organelles, we also evaluated the effect of autophagy inhibitors and activators on **12A**-induced vacuoles. The results revealed that the **12A**-induced vacuolization did not decrease when cells were pre-treated with two autophagy

inhibitors, namely 3-methyladenine (3-MA) and LY294002 (Figure 4(B)). In addition, the autophagy activator rapamycin also failed to promote the **12A**-induced vacuolization (Figure 4(B)). These results suggest that the **12A**-induced vacuoles are not the autophagic vacuoles (AVs).

Methuosis is characterised by the accumulation of cytoplasmic vacuoles derived from macropinosomes. It has been reported that protein synthesis is needed during macropinosome formation. Bafilomycin A1 (Baf-A1), a selective inhibitor of vacuolar-type H<sup>+</sup> ATPase (V-ATPase), can inhibit nascent macropinosome formation and restore the vacuoles to normal morphology by inhibiting acid influx in cells<sup>24</sup>. Cycloheximide (CHX) is a protein synthesis inhibitor that can disrupt the process of macropinosome formation<sup>24</sup>. Accordingly, HeLa cells were treated with **12A** or in combination with Baf-A1 or CHX for 8 h, and the morphological changes were then imaged. As shown in Figure 4(C), both CHX and Baf-A1 dramatically blocked the formation of vacuoles, indicating that **12A** was a methuosis inducer.

#### 2.2.4. The MAPK/JNK pathway is involved in **12A**-induced methuosis

We also examined the methuotic features of **12A**-induced vacuolization-mediated cell death. First, examination of the cells by transmission electron microscopy (TEM) revealed ER swelling after treatment with **12A** (Figure 5(A)), implying that the compound **12A**-induced cytoplasmic vacuoles may originate from the ER and be accompanied by ER stress. To evaluate whether ER stress is involved in **12A**-induced methuosis, the mRNA expression level of the endoplasmic reticulum (ER) stress marker CHOP was measured. As shown in Figure 5(B), treatment with **12A** increased the CHOP mRNA level in a dose-dependent manner. Together, these data support that **12A** induces macropinosome-derived vacuoles. Methuosis can be induced by activation of the MAPK/JNK signalling pathway and the insulin-like growth factor I receptor signalling pathway<sup>25–27</sup>. Therefore, we evaluated the levels of JNK, p-JNK, ERK1/2, and p-ERK1/2 in HeLa cells and MDA-MB-231 cells with or without **12A** treatment. The results shown in Figure 5(C) revealed that p-JNK and p-ERK1/2 were dose-dependently increased in **12A**-treated HeLa and MDA-MB-231 cells. The increase of p-JNK and p-ERK1/2 after **12A** treatment suggested that the activation of the MAPK/JNK signalling pathway was involved in **12A**-induced vacuolization. To further confirm whether the **12A**-induced vacuole formation required the activation of the MAPK/JNK signalling pathway, the effects of the MAPK/JNK inhibitors PD98059 and SP600125 were assessed. HeLa cells were pre-treated with these two inhibitors for 2 h, then treated with **12A** for 8 h. As shown in Figure 5(D), vacuolization in HeLa cells significantly decreased in the presence of MAPK/JNK inhibitors. These findings imply that the MAPK/JNK signalling pathway is involved in **12A**-induced methuosis, demonstrating that **12A**-induced vacuoles are the hallmark of methuosis.

#### 2.2.5. Compound **12A** inhibits tumour growth *in vivo*

The above experimental results imply that compound **12A** is a novel potent vacuolization-inducing agent that promotes methuosis-like cell death in different cancer cells (HeLa, HepG2, MDA-MB-231, and MCF-7), but not in normal human cells (HaCat, MCF-10A, and LO2). Remarkably, **12A** also shows a broad spectrum of cytotoxicity against cancer cells with IC<sub>50</sub> values below 6.0 μM but does not affect non-tumorigenic cell lines, like MCF-10A and LO2 (IC<sub>50</sub>>50 μM). In particular, **12A** exhibits more than

40-fold selectivity between MDA-MB-231 (IC<sub>50</sub> = 4.51 ± 0.33 μM) and MCF-10A cells (IC<sub>50</sub> = 185.7 ± 0.51 μM). Triple-negative breast cancer (TNBC) is currently one of the trickiest tumours for clinical treatment<sup>28,29</sup>. In this study, we established a TNBC xenograft model in mice based on the implantation of MDA-MB-231 cells to evaluate the *in vivo* antitumor effects of **12A**. The effects of **12A** on MDA-MB-231 cell-mediated tumour progression are shown in Figure 6(A–C). The results showed that the treatment with **12A** substantially suppressed tumour growth, achieving 72.6% (50 mg/kg, i.p.) and 57.3% (25 mg/kg, i.p.) tumour growth inhibition (TGI). Also, **12A**-treatment did not cause a significant loss of body weight (Figure 6(D)). Additionally, we investigated the effects of **12A** on tumour cell morphology using haematoxylin and eosin (H&E) staining (Figure 6(E)). The control sample contains denser packed tumour cells with normal morphological features, while in the **12A**-treated samples the tumour cells are loosely and irregularly arranged and many necrotic cells are present showing aberrant nuclear morphology, such as karyolysis and pyknosis. Furthermore, in **12A**-treated tumour tissues (especially high-dose treated samples), there is extensive severe necrosis that appears in light pink cells without colourable nuclei, and results in more interspace. Together, these findings suggest that compound **12A** has a strong anticancer effect and good tolerability *in vivo*, indicating that **12A** can be used as a potential methuosis inducer for the treatment of cancers, such as TNBC.

### 3. Conclusion

In summary, three series of pyridine-pyrimidine-indole-carbohydrazide derivatives were designed, synthesised, and evaluated for biological effects *in vitro* and *in vivo*. In HeLa cells, the majority of the synthetic analogs exhibited potential vacuolization-inducing effect at 1 μM, and/or had significant antiproliferative activity at 20 μM. We investigated the preliminary structure-activity relationship (SAR) and found four potent compounds (**12g**, **12i**, **12n**, and **12A**) that had both similar anti-proliferative and vacuole-inducing effects as MOMIPP. Besides, in HeLa cells, the representative compound **12A** induced vacuolization in the other seven cancer cell lines tested, including MDA-MB-231, but not in the three human normal cell lines tested, including MCF-10A, which was consistent with its antiproliferative activity (cancer cell lines: IC<sub>50</sub><6 μM; normal cell lines: IC<sub>50</sub>>50 μM). A subsequent mechanism study demonstrated that compound **12A** induced caspase-independent cytoplasmic vacuolization and the vacuoles were derived from macropinosomes, instead of autophagosomes. Compound **12A** was also found to induce methuosis through the MAPK/JNK signalling pathway. Furthermore, the results obtained in the MDA-MB-231 xenograft mouse model suggested that **12A** could significantly suppress the tumour growth and showed obvious accumulation of vacuoles in tumour tissues, but had almost no influence on the body weight. Taken together, our results demonstrate that **12A** acts as a methuosis inducer and has obvious anticancer effects, and lower toxicity to normal cells/tissues. Thus, **12A** is a potential candidate for the development of novel anticancer treatment strategies, especially for TNBC treatment. Moreover, **12A** can serve as a lead compound to make further structural optimisation. Our main future goals are to develop highly selective and low toxic methuosis-based anticancer agents and identify the targets of these methuosis-inducing agents.



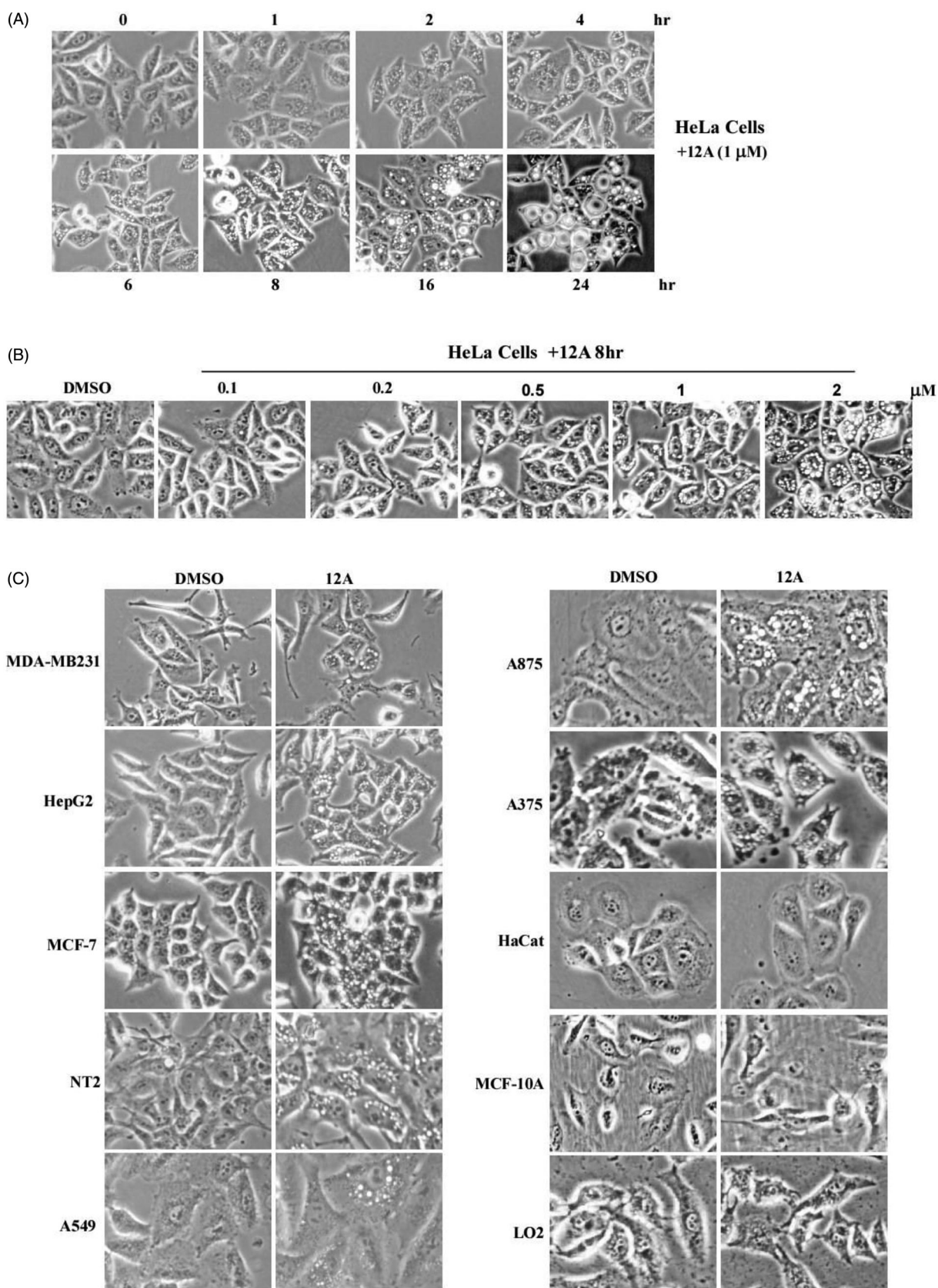


**Figure 3.** Compound 12A effectively induces cytoplasmic vacuolization in cancer cells. (A) HeLa cells were treated with 1  $\mu$ M 12A, and imaged by microscopy at the indicated time. (B) HeLa cells were treated with 12A for 8 h at the indicated concentrations, then imaged by microscopy. (C) Different cancer cells were treated with 1  $\mu$ M 12A for 8 h and normal human HaCat, MCF-10A, and LO2 cells were used as negative controls.

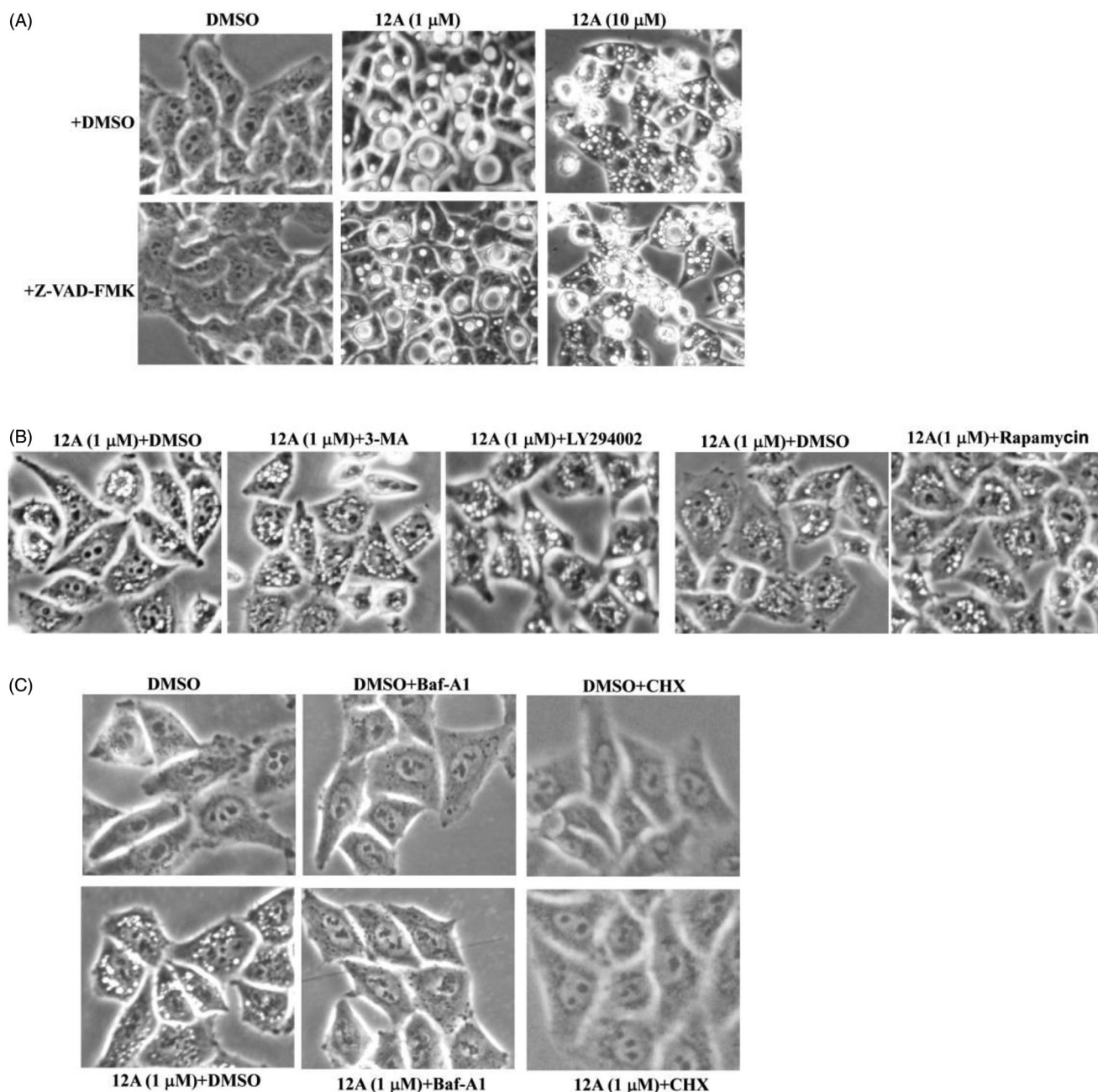


**Figure 4.** The effect of different compounds on 12A-induced vacuolation. (A) A pan-caspase inhibitor (Z-VAD-FMK). (B) Two autophagy inhibitors (3-methyladenine (3-MA) and LY294002) and an autophagy activator (rapamycin). (C) Two macropinosome formation inhibitors bafilomycin A1 (Baf-A1) and cycloheximide (CHX) were used to treat HeLa cells alone or co-treated HeLa cells treated with 12A, as indicated for 8 h, cells were imaged by microscopy.

## 4. Experimental section

### 4.1. Chemistry

All chemicals and solvents were of analytical grade, and were purchased commercially and used without further purification. All melting points were measured with a SGW X-4 micro-melting point apparatus (INESA Co., Ltd., Shanghai, China) and were uncorrected. High-resolution mass spectrometry (HRMS) was performed on a Q-Exactive mass spectrometer (Thermo Fisher Scientific Inc., Waltham, MA, USA) equipped with an electrospray ionisation source (ESI). Proton nuclear magnetic resonance ( $^1\text{H-NMR}$ ) and  $^{13}\text{C-NMR}$  spectra were performed on a Bruker Avance 600 MHz spectrometer (Bruker Biospin GmbH, Rheinstetten, Germany). The

purity of synthesised compounds was determined by high-performance liquid chromatography (HPLC) performed on an Agilent 1100 Series HPLC system (Agilent Technologies, Santa Clara, CA, USA) using a COSMOSIL5C18-MS-II Column (4.6ID  $\times$  250 mm). The mobile phase was water (A) and acetonitrile (B) in a linear gradient model as follows: (A) from 95 to 0% and (B) from 5 to 100% during 0–30 min. The flow rate was  $1\text{ ml}\cdot\text{min}^{-1}$ , and the detection wavelengths were 254 and 365 nm.

#### 4.1.1. Synthesis of intermediates 2–5

Compounds 2–5 were prepared by previously described methods<sup>29</sup>.



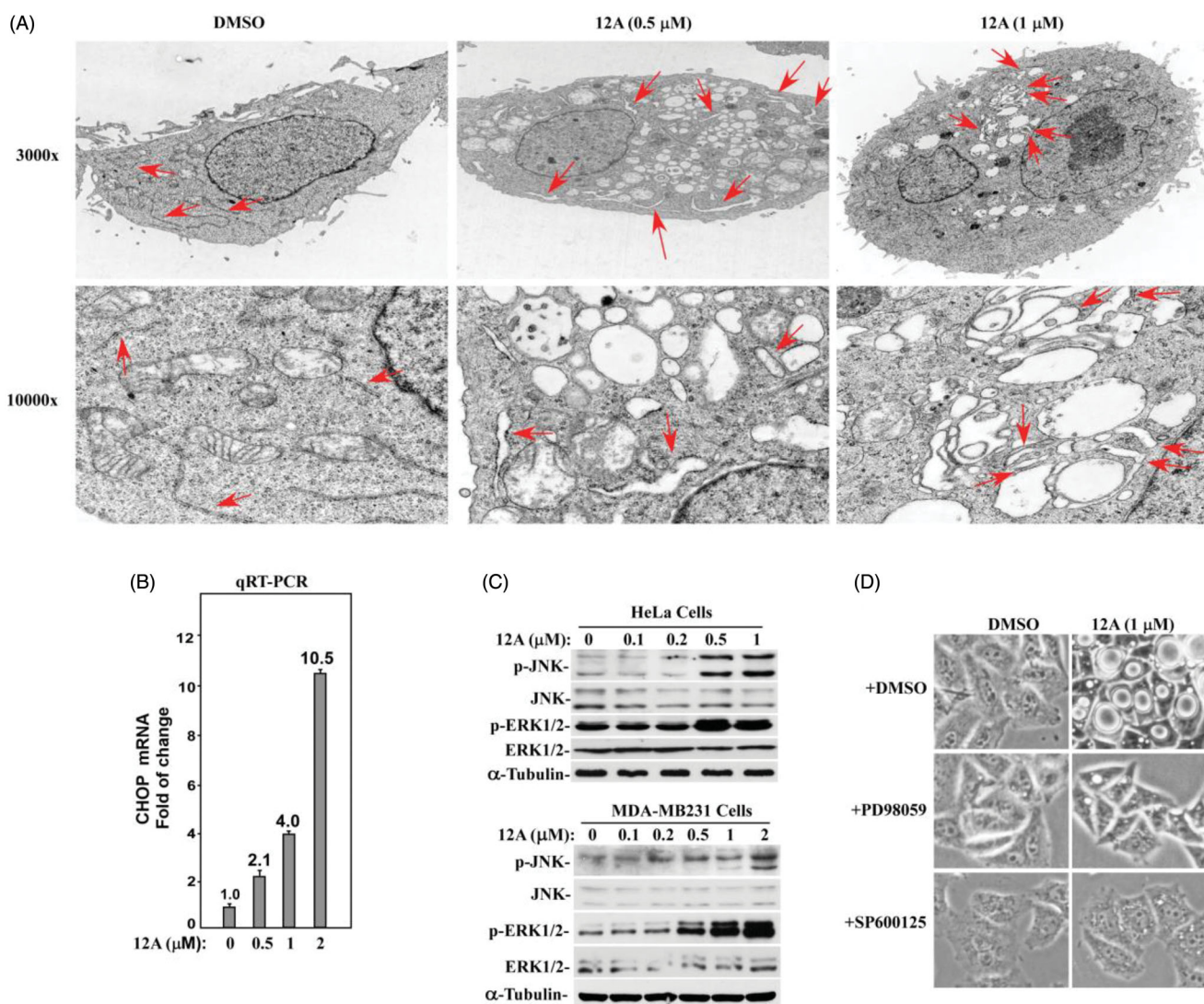


**Figure 5.** Compound 12A activates the MAPK/JNK signalling pathway and induces methuosis-like vacuoles originated from the ER and accompanied by ER stress. (A) Transmission electron microscopy (TEM) image of HeLa cells after treatment with 12A for 8 h. Red arrows: the ER (red arrows) in HeLa cells. Scale bar: 0.5 μm for 3,000x and 0.1 μm for 10,000x. (B) The CHOP mRNA levels in HeLa cells after treatment with 12A for 8 h. (C) The levels of the indicated proteins in the MAPK/JNK signalling pathway after treatment with 12A for 24 h. (D) The effect of the ERK1/2 inhibitor PD98059 and JNK inhibitor SP600125 on 12A-induced methuosis after treatment for 8 h.

#### 4.1.2. Synthesis of intermediate 6

A mixture of ethyl 5-isocyanato-1H-indole-2-carboxylate **5** (0.4 mmol, 0.092 g) in toluene (5 ml) and 6-methyl-N1-(4-(pyridin-3-yl)pyrimidin-2-yl)benzene-1,3-diamine (0.4 mmol, 0.11 g) was heated at 65 °C for 6 h. Then, the mixture was concentrated, and the resulting crude product was purified by flash chromatography on silica gel, eluting with the appropriate mixtures of CH<sub>2</sub>Cl<sub>2</sub> and MeOH to obtain intermediate **6** as a white solid with an 80% yield. <sup>1</sup>H NMR (600 MHz, DMSO-d<sub>6</sub>): δ 11.76 (s, 1H), 9.30 (s, 1H), 8.91 (s, 1H), 8.70 (d, *J* = 5.1 Hz, 1H), 8.56 (s, 1H), 8.53–8.48 (m, 3H), 7.85 (s, 1H), 7.80 (s, 1H), 7.53 (dd, *J* = 5.1, 8.1 Hz, 1H), 7.44 (d, *J* = 5.1 Hz, 1H), 7.37 (d, *J* = 8.1 Hz, 1H), 7.24 (dd, *J* = 2.0, 8.1 Hz, 1H), 7.18–7.15 (m, 1H), 7.15–7.11 (m, 1H), 7.06 (s, 1H), 4.33 (q, *J* = 7.2 Hz, 2H), 2.20 (s, 3H), 1.34 (t, *J* = 7.2 Hz, 3H); <sup>13</sup>C NMR (150 MHz, DMSO-d<sub>6</sub>): δ 162.1 (C=O), 161.7 (C=O), 60.8 (CH<sub>2</sub>), 18.0 (CH<sub>3</sub>), 14.8 (CH<sub>3</sub>), aromatic carbon atoms (23 C) gave signals at 161.6, 159.9, 153.4, 151.8, 148.7, 138.4, 134.9, 134.2, 133.2, 132.7, 130.7, 128.1, 127.3, 125.6, 124.3, 119.3, 115.1, 114.9, 113.1, 110.9, 108.0, 107.8; ESI-HRMS (+): *m/z* calcd for C<sub>28</sub>H<sub>26</sub>N<sub>7</sub>O<sub>3</sub><sup>+</sup> [M + H]<sup>+</sup>

508.2092, found 508.2090; calcd for C<sub>28</sub>H<sub>25</sub>N<sub>7</sub>O<sub>3</sub>Na<sup>+</sup> [M + Na]<sup>+</sup> 530.1911, found 530.1910.

#### 4.1.3. Synthesis of intermediate 7

A 12-ml volume of an 80% hydrazine hydrate solution was added to a solution of intermediate **6** (5 mmol, 2.54 g) in 12 ml of ethanol. Then, the mixture was refluxed for 10 h. Afterwards, the reaction mixture was filtered to obtain the intermediate **7** as white solid (85% yield). <sup>1</sup>H NMR (600 MHz, DMSO-d<sub>6</sub>): δ 11.46 (s, 1H), 9.73 (s, 1H), 9.31 (s, 1H), 8.87 (s, 1H), 8.71 (d, *J* = 5.1 Hz, 1H), 8.55–8.49 (m, 3H), 8.43 (s, 1H), 7.86 (s, 1H), 7.80 (s, 1H), 7.53 (dd, *J* = 5.1, 8.1 Hz, 1H), 7.43 (d, *J* = 5.1 Hz, 1H), 7.34 (d, *J* = 8.1 Hz, 1H), 7.16–7.09 (m, 3H), 7.01 (s, 1H), 4.49 (s, 2H), 2.21 (s, 3H); <sup>13</sup>C NMR (150 MHz, DMSO-d<sub>6</sub>): 162.0 (C=O), 161.7 (C=O), 18.0 (CH<sub>3</sub>), aromatic carbon atoms (23 C) gave signals at 161.6, 159.9, 153.4, 151.9, 148.7, 138.5, 138.4, 135.0, 133.2, 132.8, 132.7, 131.4, 130.7, 127.7, 125.4, 124.2, 117.6, 115.0, 114.8, 112.8, 110.7, 108.0, 102.1; ESI-HRMS (+): *m/z* calcd for C<sub>24</sub>H<sub>24</sub>N<sub>7</sub>O<sub>3</sub><sup>+</sup> [M + H]<sup>+</sup> 494.2047,

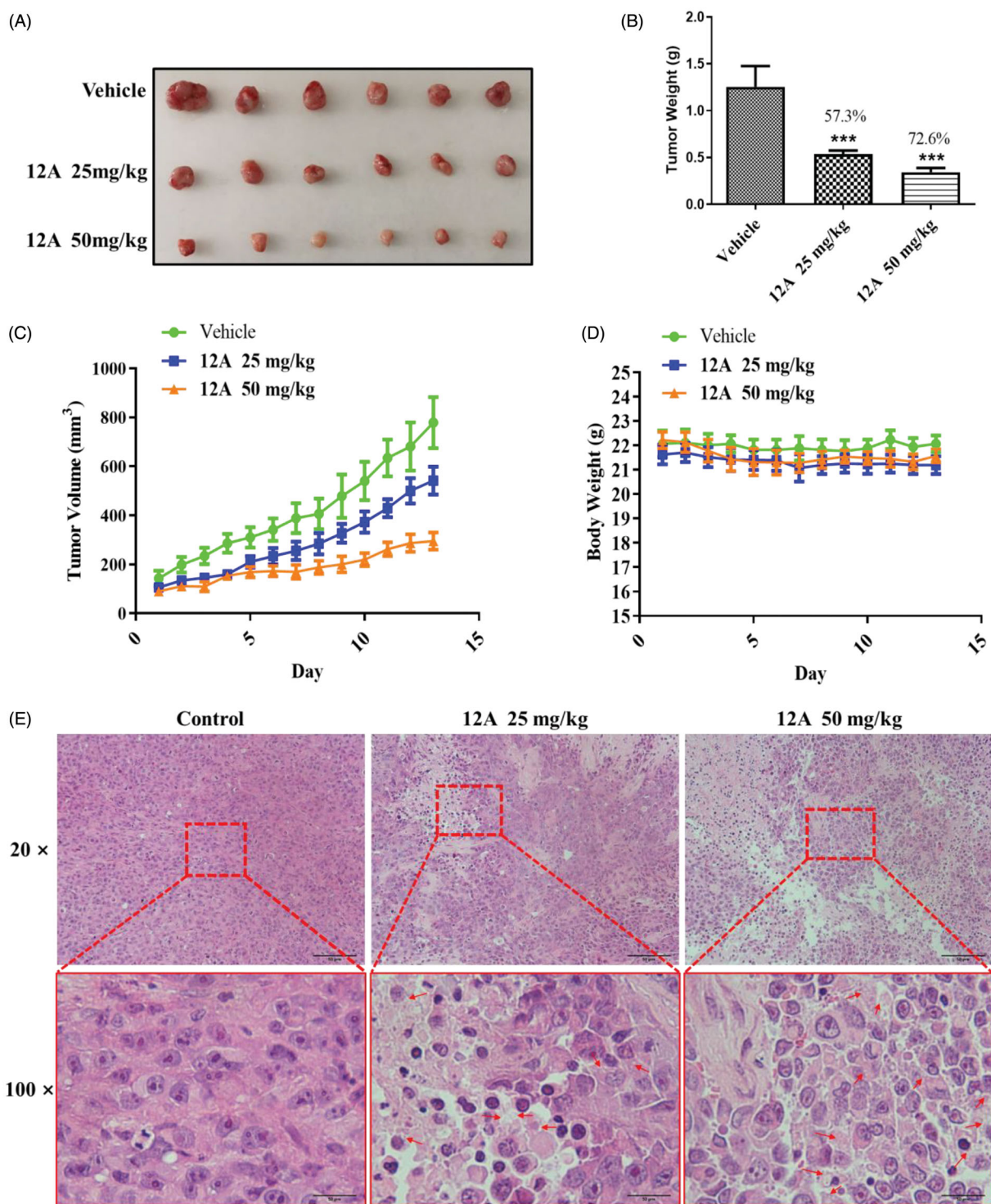


**Figure 6.** Compound 12A suppresses MDA-MB-231 tumour growth *in vivo*. (A–B) Nude mice with MDA-MB-231 xenografts were intraperitoneally (i.p.) injected daily with vehicle, 12A (25 mg/kg or 50 mg/kg) for 13 days. Tumours were separated and measured. Tumour size and weight in control and 12A-treated mice were compared. (C–D) Tumour volume and body-weight of mice during treatment. Tumour volume and body weight were measured every day. Error bars indicate mean tumour volume  $\pm$  SEM and mean body weight  $\pm$  SEM ( $n=6$  animals in each group). (E) H&E staining in untreated tumours or after 13 days of the treatment with 12A. Red arrows indicate vacuoles.

found 494.2047; calcd for  $C_{24}H_{23}N_7O_3Na^+$   $[M+Na]^+$  516.1867, found 516.1864.

#### 4.1.4. General procedure for the synthesis of compounds 8a–8f (series A)

Different aromatic aldehydes (0.4 mmol) were separately added to a solution of 5-isocyanato-1*H*-indole-adamantine **6** (0.12 g, 0.4 mmol) in 5 ml of toluene. The mixtures were heated at 60 °C



for 4 h. Subsequently, the reaction mixtures were concentrated and the resulting crudes were purified by flash chromatography on silica gel, eluting with the appropriate mixtures of  $\text{CH}_2\text{Cl}_2$  and MeOH to afford the corresponding target compounds **8a–8f**. Their structures were characterised by NMR and ESI-HRMS. The structures and IUPAC names of these target compounds (Series A) are listed in Table S1 (Supporting Information).

**Compound 8a:** Yellow solid; Yield: 81%; HPLC purity: 95.37%;  $^1\text{H}$  NMR (600 MHz,  $\text{DMSO-d}_6$ ):  $\delta$  11.62 (s, 1H), 11.43 (s, 1H), 9.30 (s, 1H), 8.88 (s, 1H), 8.71 (d,  $J=3.9$  Hz, 1H), 8.54 (s, 1H), 8.53–8.50 (m, 2H), 8.46 (s, 1H), 7.89–7.83 (m, 2H), 7.74 (s, 1H), 7.53 (dd,  $J=5.1$ , 8.1 Hz, 1H), 7.43 (d,  $J=5.1$  Hz, 1H), 7.36 (d,  $J=8.1$  Hz, 1H), 7.20–7.06 (m, 4H), 2.33–2.23 (m, 2H), 2.21 (s, 3H), 1.54 (d,  $J=8.1$  Hz, 2H), 0.95 (t,  $J=7.3$  Hz, 3H);  $^{13}\text{C}$  NMR (150 MHz,  $\text{DMSO-d}_6$ ):  $\delta$  162.1 (C=O), 161.6 (C=O), 148.7 (–CH=N), 56.0 ( $\text{CH}_2$ ), 55.9 ( $\text{CH}_2$ ), 40.4 ( $\text{CH}_3$ ), 18.0 ( $\text{CH}_3$ ), aromatic carbon atoms (23 C) gave signals at 159.9, 153.4, 151.9, 151.2, 149.5, 147.9, 138.4, 135.0, 133.1, 132.7, 130.7, 127.6, 127.5, 125.5, 124.3, 122.4, 115.1, 114.8, 113.0, 111.9, 108.6, 108.0, 103.6; ESI-HRMS (+):  $m/z$  calcd for  $\text{C}_{30}\text{H}_{30}\text{N}_9\text{O}_2^+$  [M + H] $^+$  548.2517, found 548.2519.

**Compound 8b:** Yellow solid; Yield: 84%; HPLC purity: 94.57%;  $^1\text{H}$  NMR (600 MHz,  $\text{DMSO-d}_6$ ):  $\delta$  11.87 (s, 1H), 11.71 (s, 1H), 9.31 (s, 1H), 8.89 (s, 1H), 8.71 (s, 1H), 8.55 (s, 1H), 8.54–8.50 (m, 2H), 8.49 (s, 2H), 7.92 (s, 1H), 7.86 (s, 1H), 7.77 (d,  $J=8.1$  Hz, 2H), 7.53 (dd,  $J=5.1$ , 8.1 Hz, 1H), 7.47 (dd,  $J=5.1$ , 8.1 Hz, 3H), 7.44 (d,  $J=5.1$  Hz, 1H), 7.40 (d,  $J=8.1$  Hz, 1H), 7.25 (s, 1H), 7.20–7.13 (m, 3H), 2.21 (s, 3H);  $^{13}\text{C}$  NMR (150 MHz,  $\text{DMSO-d}_6$ ):  $\delta$  162.1 (C=O), 161.6 (C=O), 148.7 (–CH=N), 18.0 ( $\text{CH}_3$ ), aromatic carbon atoms (27 C) gave signals at 159.9, 154.9, 153.5, 151.8, 151.3, 138.4, 137.6, 136.7, 134.9, 134.3, 132.7, 130.9, 130.8, 130.7, 130.7, 130.5, 127.5, 125.5, 124.2, 120.3, 115.1, 114.9, 113.0, 108.8, 108.5, 108.0, 94.7; ESI-HRMS (+):  $m/z$  calcd for  $\text{C}_{33}\text{H}_{28}\text{N}_9\text{O}_2^+$  [M + H] $^+$  582.2360, found 582.2363.

**Compound 8c:** Yellow solid; Yield: 83%; HPLC purity: 97.32%;  $^1\text{H}$  NMR (600 MHz,  $\text{DMSO-d}_6$ ):  $\delta$  11.83 (s, 1H), 11.69 (s, 1H), 9.31 (s, 1H), 8.89 (s, 1H), 8.71 (s, 1H), 8.68 (s, 1H), 8.56 (s, 1H), 8.54–8.50 (m, 2H), 8.49 (s, 1H), 7.91 (s, 1H), 7.86 (s, 1H), 7.68 (s, 1H), 7.53 (dd,  $J=5.1$ , 8.1 Hz, 1H), 7.49 (brs, 1H), 7.43 (d,  $J=5.1$  Hz, 1H), 7.40 (d,  $J=8.1$  Hz, 1H), 7.21 (s, 1H), 7.19–7.12 (m, 4H), 2.21 (s, 3H);  $^{13}\text{C}$  NMR (150 MHz,  $\text{DMSO-d}_6$ ):  $\delta$  162.1 (C=O), 161.6 (C=O), 148.7 (–CH=N), 18.0 ( $\text{CH}_3$ ), aromatic carbon atoms (27 C) gave signals at 159.9, 158.0, 153.4, 151.8, 142.7, 139.6, 138.4, 135.0, 133.7, 133.1, 132.7, 131.4, 130.9, 130.7, 129.4, 128.4, 127.6, 125.5, 124.3, 120.6, 118.4, 115.1, 114.9, 113.0, 110.8, 108.0, 103.8; ESI-HRMS (+):  $m/z$  calcd for  $\text{C}_{31}\text{H}_{26}\text{N}_9\text{O}_2\text{S}^+$  [M + H] $^+$  588.1925, found 588.1926.

**Compound 8d:** Yellow solid; Yield: 80%; HPLC purity: 97.02%;  $^1\text{H}$  NMR (600 MHz,  $\text{DMSO-d}_6$ ):  $\delta$  12.04 (s, 1H), 11.72 (s, 1H), 9.31 (s, 1H), 8.89 (s, 2H), 8.71 (s, 1H), 8.64 (s, 1H), 8.57 (s, 1H), 8.53 (d,  $J=5.1$  Hz, 3H), 8.50 (s, 1H), 8.19 (d,  $J=5.1$  Hz, 1H), 7.92 (s, 1H), 7.85 (s, 1H), 7.53 (d,  $J=5.1$  Hz, 2H), 7.44 (d,  $J=5.1$  Hz, 1H), 7.40 (d,  $J=8.1$  Hz, 1H), 7.26 (s, 1H), 7.18 (d,  $J=8.1$  Hz, 1H), 7.15 (s, 2H), 2.21 (s, 3H);  $^{13}\text{C}$  NMR (150 MHz,  $\text{DMSO-d}_6$ ):  $\delta$  164.5 (C=O), 162.0 (C=O), 148.6 (–CH=N), 18.0 ( $\text{CH}_3$ ), aromatic carbon atoms (27 C) gave signals at 162.0, 161.6, 161.1, 159.9, 153.5, 151.7, 150.9, 149.0, 144.7, 140.0, 135.1, 134.1, 133.8, 133.1, 132.8, 130.7, 128.9, 127.6, 125.5, 124.5, 124.3, 115.1, 118.7, 114.9, 113.0, 110.9, 108.0; ESI-HRMS (–):  $m/z$  calcd for  $\text{C}_{32}\text{H}_{25}\text{N}_{10}\text{O}_2^-$  [M–H] $^-$  581.2167, found 581.2181.

**Compound 8e:** Yellow solid; Yield: 86%; HPLC purity: 96.39%;  $^1\text{H}$  NMR (600 MHz,  $\text{DMSO-d}_6$ ):  $\delta$  11.73 (s, 1H), 11.67 (s, 1H), 9.30 (s, 1H), 8.89 (s, 1H), 8.71 (s, 1H), 8.55 (s, 1H), 8.54–8.50 (m, 2H), 8.47 (s, 1H), 8.41 (s, 1H), 7.90 (s, 1H), 7.85 (s, 1H), 7.71 (d,  $J=8.1$  Hz, 2H), 7.53 (dd,  $J=5.1$ , 8.1 Hz, 1H), 7.44 (d,  $J=5.1$  Hz, 1H), 7.39 (d,  $J=8.1$  Hz, 1H), 7.21 (brs, 1H), 7.18–7.11 (m, 3H), 7.04 (d,  $J=8.1$  Hz,

2H), 3.82 (s, 3H), 2.21 (s, 3H);  $^{13}\text{C}$  NMR (150 MHz,  $\text{DMSO-d}_6$ ):  $\delta$  162.1 (C=O), 161.6 (C=O), 148.7 (–CH=N), 55.8 (OCH<sub>3</sub>), 18.0 ( $\text{CH}_3$ ), aromatic carbon atoms (25 C) gave signals at 161.3, 159.9, 157.9, 153.4, 151.8, 147.5, 138.4, 135.0, 133.6, 133.0, 132.7, 131.1, 130.7, 129.2, 127.6, 127.4, 125.5, 124.3, 118.3, 115.1, 114.9, 114.8, 113.0, 110.8, 108.0, 103.6; ESI-HRMS (+):  $m/z$  calcd for  $\text{C}_{34}\text{H}_{30}\text{N}_9\text{O}_3^+$  [M + H] $^+$  612.2466, found 612.2467.

**Compound 8f:** Yellow solid; Yield: 89%; HPLC purity: 93.88%;  $^1\text{H}$  NMR (600 MHz,  $\text{DMSO-d}_6$ ):  $\delta$  11.74 (s, 1H), 11.65 (s, 1H), 9.30 (s, 1H), 8.89 (s, 1H), 8.71 (s, 1H), 8.54 (s, 1H), 8.53–8.50 (m, 2H), 8.47 (s, 1H), 8.39 (s, 1H), 7.89 (s, 1H), 7.84 (s, 1H), 7.53 (dd,  $J=5.1$ , 8.1 Hz, 1H), 7.44 (d,  $J=5.1$  Hz, 1H), 7.41–7.35 (m, 2H), 7.28–7.20 (m, 2H), 7.18–7.12 (m, 3H), 7.05 (d,  $J=8.1$  Hz, 1H), 3.85 (s, 3H), 3.82 (s, 3H), 2.21 (s, 3H);  $^{13}\text{C}$  NMR (150 MHz,  $\text{DMSO-d}_6$ ):  $\delta$  162.1 (C=O), 161.6 (C=O), 148.7 (–CH=N), 56.1 (OCH<sub>3</sub>), 56.0 (OCH<sub>3</sub>), 18.0 ( $\text{CH}_3$ ), aromatic carbon atoms (29 C) gave signals at 159.9, 157.9, 153.4, 151.8, 151.2, 149.6, 147.9, 138.4, 134.9, 133.6, 133.0, 132.7, 131.0, 130.7, 127.6, 127.6, 127.5, 125.5, 124.3, 122.4, 118.3, 115.1, 114.9, 112.9, 112.0, 110.8, 108.7, 108.0, 103.6; ESI-HRMS (+):  $m/z$  calcd for  $\text{C}_{35}\text{H}_{32}\text{N}_9\text{O}_4^+$  [M + H] $^+$  642.2572, found 642.2573.

#### 4.1.5. Synthesis of intermediates 10 and 11

The intermediates **10** and **11** were synthesised as previously described<sup>20</sup>.

#### 4.1.6. General procedure for the synthesis of compounds 12a–12r (series B)

The mixtures of different aldehydes (1.2 mmol) and **11** (0.345 g, 1 mmol) in ethyl 5 ml of ethanol were heated to reflux for 8 h. The solvent was removed from the reaction mixtures under a vacuum. The resulting crude products were purified by flash chromatography on silica gel, eluting with the appropriate mixtures of  $\text{CH}_2\text{Cl}_2$  and MeOH to obtain the corresponding compounds **12a–12r**. Their structures were characterised by NMR and ESI-HRMS. Structures and IUPAC names of these target compounds (Series B) are listed in Table S2 (Supporting Information).

**Compound 12a:** Yellow solid; Yield: 91%; HPLC purity: 95.78%;  $^1\text{H}$ -NMR (600 MHz,  $\text{DMSO-d}_6$ ):  $\delta$  11.68 (s, 1H), 11.48 (s, 1H), 9.60 (s, 1H), 9.37 (s, 1H), 8.74 (s, 1H), 8.58 (s, 1H), 8.50 (d,  $J=5.1$  Hz, 1H), 8.20 (s, 1H), 7.77 (s, 1H), 7.59 (s, 1H), 7.51 (s, 1H), 7.43 (s, 2H), 7.20 (s, 1H), 1.97 (s, 3H);  $^{13}\text{C}$ -NMR (150 MHz,  $\text{DMSO-d}_6$ ):  $\delta$  161.9 (C=O), 148.6 (–CH=N), 19.0 ( $\text{CH}_3$ ), aromatic carbon atoms (17 C) gave signals at 161.1, 159.8, 157.8, 151.9, 148.0, 134.8, 133.6, 133.6, 132.9, 131.0, 127.4, 124.4, 119.4, 112.6, 111.6, 107.9, 103.4; ESI-HRMS (+):  $m/z$  calcd for  $\text{C}_{20}\text{H}_{18}\text{N}_7\text{O}^+$  [M + H] $^+$  372.1567, found 372.1565,  $\text{C}_{20}\text{H}_{17}\text{N}_7\text{ONa}^+$  [M + Na] $^+$  394.1387, found 394.1385.

**Compound 12b:** Yellow solid; Yield: 90%; HPLC purity: 93.70%;  $^1\text{H}$ -NMR (600 MHz,  $\text{DMSO-d}_6$ ):  $\delta$  11.66 (s, 1H), 11.50–11.36 (m, 1H), 9.59 (s, 1H), 9.35 (s, 1H), 8.72 (s, 1H), 8.56 (d,  $J=2.1$  Hz, 1H), 8.48 (d,  $J=5.1$  Hz, 1H), 8.19 (s, 1H), 7.77 (s, 1H), 7.57 (s, 1H), 7.51 (d,  $J=5.1$  Hz, 1H), 7.46–7.34 (m, 1H), 7.19 (s, 1H), 2.31 (s, 2H), 1.05 (t,  $J=7.1$  Hz, 3H);  $^{13}\text{C}$ -NMR (150 MHz,  $\text{DMSO-d}_6$ ):  $\delta$  161.9 (C=O), 148.6 (–CH=N), 25.9 ( $\text{CH}_2$ ), 11.2 ( $\text{CH}_3$ ), aromatic carbon atoms (17 C) gave signals at 161.1, 159.8, 157.9, 152.8, 151.9, 134.8, 133.6, 133.6, 132.9, 131.0, 127.4, 124.3, 119.4, 112.6, 111.6, 107.9, 103.6; ESI-HRMS (+):  $m/z$  calcd for  $\text{C}_{21}\text{H}_{20}\text{N}_7\text{O}^+$  [M + H] $^+$  386.1724, found 386.1719,  $\text{C}_{21}\text{H}_{19}\text{N}_7\text{ONa}^+$  [M + Na] $^+$  408.1543, found 408.1540.

**Compound 12c:** Yellow solid; Yield: 89%; HPLC purity: 96.70%;  $^1\text{H}$ -NMR (600 MHz,  $\text{DMSO-d}_6$ ):  $\delta$  11.67 (s, 1H), 11.46 (s, 1H), 9.60 (s, 1H), 9.37 (s, 1H), 8.74 (s, 1H), 8.58 (s, 1H), 8.50 (d,  $J=5.1$  Hz, 1H), 8.20 (s, 1H), 7.75 (s, 1H), 7.59 (s, 1H), 7.51 (d,  $J=5.1$  Hz, 1H),



7.47–7.37 (m, 2H), 7.20 (s, 1H), 2.28 (s, 2H), 1.56 (s, 2H), 0.96 (s, 3H);  $^{13}\text{C-NMR}$  (150 MHz,  $\text{DMSO-d}_6$ ):  $\delta$  161.9 (C=O), 148.6 (–CH=N), 33.6 ( $\text{CH}_2$ ), 20.6 ( $\text{CH}_2$ ), 14.1 ( $\text{CH}_3$ ), aromatic carbon atoms (17C) gave signals at 161.1, 159.8, 157.9, 151.9, 134.8, 133.6, 133.5, 132.9, 131.0, 127.4, 124.3, 119.4, 112.6, 111.6, 107.9, 103.5; ESI-HRMS (+):  $m/z$  calcd for  $\text{C}_{22}\text{H}_{22}\text{N}_7\text{O}^+$  [M + H] $^+$  400.1880, found 400.1877,  $\text{C}_{22}\text{H}_{21}\text{N}_7\text{ONa}^+$  [M + Na] $^+$  422.1700, found 420.1696.

**Compound 12d:** Yellow solid; Yield: 86%; HPLC purity: 95.45%;  $^1\text{H-NMR}$  (600 MHz,  $\text{DMSO-d}_6$ ):  $\delta$  11.91 (s, 1H), 11.77 (s, 1H), 9.64 (s, 1H), 9.38 (s, 1H), 8.75 (s, 1H), 8.59 (d,  $J=3.1$  Hz, 1H), 8.54–8.44 (m, 2H), 8.25 (s, 1H), 7.77 (s, 2H), 7.60 (s, 1H), 7.53 (s, 1H), 7.51–7.39 (m, 5H), 7.31 (s, 1H);  $^{13}\text{C-NMR}$  (150 MHz,  $\text{DMSO-d}_6$ ):  $\delta$  163.3 (C=O), 148.6 (–CH=N), aromatic carbon atoms (23C) gave signals at 161.9, 161.1, 159.9, 158.1, 151.9, 147.4, 145.4, 136.9, 134.9, 134.8, 133.7, 132.9, 132.3, 130.8, 130.5, 129.3, 127.5, 124.4, 119.6, 112.7, 111.6, 107.9, 104.0; ESI-HRMS (+):  $m/z$  calcd for  $\text{C}_{25}\text{H}_{20}\text{N}_7\text{O}^+$  [M + H] $^+$  434.1724, found 434.1718; calcd for  $\text{C}_{25}\text{H}_{19}\text{N}_7\text{ONa}^+$  [M + Na] $^+$  456.1543, found 456.1537.

**Compound 12e:** This compound has been reported in our previous work<sup>16</sup>.

**Compound 12f:** Yellow solid; Yield: 89%; HPLC purity: 94.45%;  $^1\text{H-NMR}$  (600 MHz,  $\text{DMSO-d}_6$ ):  $\delta$  12.15 (s, 1H), 11.78 (s, 1H), 11.24 (s, 1H), 9.71 (s, 1H), 9.43 (s, 1H), 8.84 (s, 1H), 8.73–8.66 (m, 2H), 8.62 (d,  $J=5.1$  Hz, 1H), 8.20 (s, 1H), 7.77 (s, 1H), 7.60 (d,  $J=5.1$  Hz, 1H), 7.56 (d,  $J=8.1$  Hz, 1H), 7.49 (d,  $J=5.1$  Hz, 1H), 7.46 (d,  $J=8.1$  Hz, 1H), 7.32 (s, 2H), 6.97 (d,  $J=8.1$  Hz, 2H);  $^{13}\text{C-NMR}$  (150 MHz,  $\text{DMSO-d}_6$ ):  $\delta$  161.2 (C=O), 147.7 (–CH=N), aromatic carbon atoms (23C) gave signals at 160.9, 159.9, 159.0, 157.9, 157.8, 149.9, 146.8, 137.1, 133.9, 133.7, 133.6, 131.8, 130.5, 129.7, 127.5, 125.3, 119.9, 119.8, 119.4, 116.9, 112.8, 112.0, 108.0, 104.2; ESI-HRMS (+):  $m/z$  calcd for  $\text{C}_{25}\text{H}_{20}\text{N}_7\text{O}_2^+$  [M + H] $^+$  450.1673, found 450.1672,  $\text{C}_{25}\text{H}_{19}\text{N}_7\text{O}_2\text{Na}^+$  [M + Na] $^+$  472.1492, found 472.1492.

**Compound 12g:** Yellow solid; Yield: 88%; HPLC purity: 96.34%;  $^1\text{H-NMR}$  (600 MHz,  $\text{DMSO-d}_6$ ):  $\delta$  11.95 (s, 1H), 11.74 (s, 1H), 9.63 (s, 1H), 9.37 (d,  $J=2.0$  Hz, 1H), 8.84 (s, 1H), 8.74 (d,  $J=5.1$  Hz, 1H), 8.58 (d,  $J=5.1$  Hz, 1H), 8.50 (td,  $J=2.0, 8.1$  Hz, 1H), 8.23 (s, 1H), 7.91 (d,  $J=8.1$  Hz, 1H), 7.59 (dd,  $J=5.1, 8.1$  Hz, 1H), 7.54 (d,  $J=8.1$  Hz, 1H), 7.47–7.40 (m, 3H), 7.34 (s, 1H), 7.12 (d,  $J=8.1$  Hz, 1H), 7.04 (t,  $J=8.1$  Hz, 1H), 3.89 (s, 3H);  $^{13}\text{C-NMR}$  (150 MHz,  $\text{DMSO-d}_6$ ):  $\delta$  161.9 (C=O), 161.1, 159.8, 158.2, 158.0, 151.9, 148.6 (–CH=N), 56.2 ( $\text{CH}_3\text{O}$ ), aromatic carbon atoms (23C) gave signals at 142.8, 134.8, 133.7, 132.9, 131.9, 130.9, 127.5, 126.0, 124.4, 122.9, 121.2, 119.6, 116.6, 112.7, 112.3, 111.6, 107.9, 104.0; ESI-HRMS (+):  $m/z$  calcd for  $\text{C}_{26}\text{H}_{22}\text{N}_7\text{O}_2^+$  [M + H] $^+$  464.1829, found 464.1828; calcd for  $\text{C}_{26}\text{H}_{21}\text{N}_7\text{O}_2\text{Na}^+$  [M + Na] $^+$  486.1649, found 486.1649.

**Compound 12h:** Yellow solid; Yield: 88%; HPLC purity: 94.11%;  $^1\text{H-NMR}$  (600 MHz,  $\text{DMSO-d}_6$ ):  $\delta$  11.77 (s, 1H), 11.73 (s, 1H), 9.62 (s, 1H), 9.38 (s, 1H), 8.74 (d,  $J=5.1$  Hz, 1H), 8.59 (d,  $J=5.1$  Hz, 1H), 8.51 (d,  $J=8.1$  Hz, 1H), 8.43 (s, 1H), 8.24 (s, 1H), 7.72 (d,  $J=8.1$  Hz, 2H), 7.63–7.49 (m, 3H), 7.44 (d,  $J=5.1$  Hz, 2H), 7.17–6.96 (m, 2H), 3.83 (s, 3H);  $^{13}\text{C-NMR}$  (150 MHz,  $\text{DMSO-d}_6$ ):  $\delta$  161.9 (C=O), 148.6 (–CH=N), 55.8 ( $\text{CH}_3\text{O}$ ), aromatic carbon atoms (21C) gave signals at 161.3, 161.1, 159.8, 151.9, 134.8, 133.7, 133.2, 132.9, 131.3, 129.1, 127.4, 119.5, 114.8, 112.7, 112.5, 111.6, 107.8, 103.7, 102.3; ESI-HRMS (+):  $m/z$  calcd for  $\text{C}_{26}\text{H}_{22}\text{N}_7\text{O}_2^+$  [M + H] $^+$  464.1829, found 464.1833,  $\text{C}_{26}\text{H}_{21}\text{N}_7\text{O}_2\text{Na}^+$  [M + Na] $^+$  486.1649, found 486.1653.

**Compound 12i:** Yellow solid; Yield: 88%; HPLC purity: 96.10%;  $^1\text{H-NMR}$  (600 MHz,  $\text{DMSO-d}_6$ ):  $\delta$  11.82 (s, 1H), 11.73 (s, 1H), 9.62 (s, 1H), 9.38 (s, 1H), 8.75 (d,  $J=5.1$  Hz, 1H), 8.59 (d,  $J=5.1$  Hz, 1H),

8.51 (d,  $J=8.1$  Hz, 1H), 8.44 (s, 1H), 8.24 (s, 1H), 7.66 (d,  $J=8.1$  Hz, 2H), 7.59 (dd,  $J=5.1, 8.1$  Hz, 1H), 7.54 (d,  $J=8.1$  Hz, 1H), 7.45 (d,  $J=5.1$  Hz, 2H), 7.30 (s, 3H), 2.37 (s, 3H);  $^{13}\text{C-NMR}$  (150 MHz,  $\text{DMSO-d}_6$ ):  $\delta$  161.9 (C=O), 148.6 (–CH=N), 21.0 ( $\text{CH}_3$ ), aromatic carbon atoms (21C) gave signals at 161.1, 159.8, 158.0, 152.0, 147.5, 140.1, 134.8, 133.7, 133.0, 132.0, 131.0, 129.9, 127.4, 124.3, 119.7, 112.7, 111.6, 107.8, 102.9; ESI-HRMS (+):  $m/z$  calcd for  $\text{C}_{26}\text{H}_{22}\text{N}_7\text{O}^+$  [M + H] $^+$  448.1880, found 448.1882, calcd for  $\text{C}_{26}\text{H}_{21}\text{N}_7\text{ONa}^+$  [M + Na] $^+$  470.1700, found 470.1705.

**Compound 12j:** Yellow solid; Yield: 86%; HPLC purity: 93.10%;  $^1\text{H-NMR}$  (600 MHz,  $\text{DMSO-d}_6$ ):  $\delta$  11.93 (s, 1H), 11.74 (s, 1H), 9.68 (s, 1H), 9.41 (s, 1H), 8.80 (d,  $J=5.1$  Hz, 1H), 8.67–8.58 (m, 2H), 8.47 (s, 1H), 8.21 (brs, 1H), 7.70 (dd,  $J=5.1, 8.1$  Hz, 1H), 7.55 (d,  $J=8.1$  Hz, 1H), 7.51 (s, 2H), 7.47 (d,  $J=5.1$  Hz, 1H), 7.46–7.42 (m, 3H), 7.40 (s, 1H), 7.31 (s, 1H), 7.20 (t,  $J=7.3$  Hz, 1H), 7.10 (d,  $J=8.1$  Hz, 3H);  $^{13}\text{C-NMR}$  (150 MHz,  $\text{DMSO-d}_6$ ):  $\delta$  161.5 (C=O), 148.4 (–CH=N), 69.8 ( $\text{CH}_2$ ), aromatic carbon atoms (29C) gave signals at 161.0, 159.9, 157.7, 156.8, 150.6, 147.4, 146.7, 136.9, 136.2, 133.8, 133.6, 133.4, 131.1, 130.7, 127.4, 124.9, 124.3, 123.2, 120.7, 119.8, 119.4, 116.3, 112.7, 111.8, 108.0, 104.1; ESI-HRMS (+):  $m/z$  calcd for  $\text{C}_{32}\text{H}_{26}\text{N}_7\text{O}_2^+$  [M + H] $^+$  540.2142, found 540.2139; calcd for  $\text{C}_{32}\text{H}_{25}\text{N}_7\text{O}_2\text{Na}^+$  [M + Na] $^+$  562.1962, found 562.1959.

**Compound 12k:** Yellow solid; Yield: 85%; HPLC purity: 93.15%;  $^1\text{H-NMR}$  (600 MHz,  $\text{DMSO-d}_6$ ):  $\delta$  11.74 (s, 2H), 9.71 (s, 1H), 9.42 (d,  $J=2.0$  Hz, 1H), 8.84 (d,  $J=5.1$  Hz, 1H), 8.70 (d,  $J=8.1$  Hz, 1H), 8.62 (d,  $J=5.1$  Hz, 1H), 8.33 (s, 1H), 8.18 (s, 1H), 7.80–7.69 (m, 1H), 7.54 (d,  $J=8.1$  Hz, 1H), 7.49 (d,  $J=5.1$  Hz, 1H), 7.44 (d,  $J=8.1$  Hz, 1H), 7.32 (s, 1H), 7.28 (s, 1H), 7.10 (d,  $J=8.1$  Hz, 1H), 7.00 (d,  $J=8.1$  Hz, 1H), 3.83 (s, 3H);  $^{13}\text{C-NMR}$  (150 MHz,  $\text{DMSO-d}_6$ ):  $\delta$  160.9 (C=O), 148.3 (–CH=N), 56.0 ( $\text{CH}_3\text{O}$ ), aromatic carbon atoms (23C) gave signals at 159.9, 159.0, 158.7, 157.9, 150.2, 149.9, 147.4, 146.7, 137.1, 133.8, 133.7, 133.5, 131.1, 127.7, 127.5, 125.3, 120.7, 112.7, 112.7, 112.3, 111.9, 108.0, 103.7; ESI-HRMS (+):  $m/z$  calcd for  $\text{C}_{26}\text{H}_{22}\text{N}_7\text{O}_3^+$  [M + H] $^+$  480.1779, found 480.1778; calcd for  $\text{C}_{26}\text{H}_{21}\text{N}_7\text{O}_3\text{Na}^+$  [M + Na] $^+$  502.1598, found 502.1596.

**Compound 12l:** Yellow solid; Yield: 91%; HPLC purity: 97.09%;  $^1\text{H-NMR}$  (600 MHz,  $\text{DMSO-d}_6$ ):  $\delta$  11.93 (s, 1H), 11.76 (s, 1H), 9.72 (s, 1H), 9.44 (d,  $J=5.1$  Hz, 1H), 8.87 (d,  $J=5.1$  Hz, 1H), 8.76 (s, 2H), 8.63 (d,  $J=5.1$  Hz, 1H), 8.18 (s, 1H), 7.83 (dd,  $J=5.1, 8.1$  Hz, 1H), 7.55 (dd,  $J=5.1, 8.1$  Hz, 1H), 7.53–7.49 (m, 2H), 7.45 (d,  $J=8.1$  Hz, 1H), 7.33 (s, 1H), 7.19–7.11 (m, 2H), 3.86 (s, 3H), 3.84 (s, 3H);  $^{13}\text{C-NMR}$  (150 MHz,  $\text{DMSO-d}_6$ ):  $\delta$  161.0 (C=O), 148.4 (–CH=N), 61.7 ( $\text{CH}_3\text{O}$ ), 56.2 ( $\text{CH}_3\text{O}$ ), aromatic carbon atoms (23C) gave signals at 160.9, 159.9, 159.0, 158.7, 153.2, 149.2, 146.1, 143.0, 137.8, 134.0, 133.4, 128.3, 127.5, 125.6, 124.8, 119.8, 117.5, 116.9, 115.0, 114.6, 112.7, 108.1, 104.0; ESI-HRMS (+):  $m/z$  calcd for  $\text{C}_{27}\text{H}_{24}\text{N}_7\text{O}_3^+$  [M + H] $^+$  494.1935, found 494.1938; calcd for  $\text{C}_{27}\text{H}_{23}\text{N}_7\text{O}_3\text{Na}^+$  [M + Na] $^+$  516.1755, found 516.1758.

**Compound 12m:** Yellow solid; Yield: 91%; HPLC purity: 95.14%;  $^1\text{H-NMR}$  (600 MHz,  $\text{DMSO-d}_6$ ):  $\delta$  11.75 (s, 1H), 11.70 (s, 1H), 9.68 (s, 1H), 9.42 (s, 1H), 8.83 (dd,  $J=2.0, 5.1$  Hz, 1H), 8.73 (s, 1H), 8.69 (d,  $J=8.1$  Hz, 1H), 8.62 (d,  $J=5.1$  Hz, 1H), 8.16 (s, 1H), 7.84 (d,  $J=8.1$  Hz, 1H), 7.77 (dd,  $J=5.1, 8.1$  Hz, 1H), 7.54 (d,  $J=8.1$  Hz, 1H), 7.49 (d,  $J=5.1$  Hz, 1H), 7.44 (d,  $J=8.1$  Hz, 1H), 7.30 (s, 1H), 6.83–6.56 (m, 2H), 3.90 (s, 3H), 3.84 (s, 3H);  $^{13}\text{C-NMR}$  (150 MHz,  $\text{DMSO-d}_6$ ):  $\delta$  162.9 (C=O), 146.8 (–CH=N), 56.3 ( $\text{CH}_3\text{O}$ ), 55.9 ( $\text{CH}_3\text{O}$ ), aromatic carbon atoms (23C) gave signals at 161.2, 161.0, 159.9, 159.6, 158.9, 158.7, 157.8, 149.9, 137.0, 133.8, 133.7, 133.4, 131.1, 127.5, 127.1, 125.2, 119.6, 115.7, 112.7, 112.0, 108.0, 106.9, 103.7; ESI-HRMS (+):  $m/z$  calcd for  $\text{C}_{27}\text{H}_{24}\text{N}_7\text{O}_3^+$  [M + H] $^+$  494.1935,

found 494.1935; calcd for  $C_{27}H_{23}N_7O_3Na^+$   $[M+Na]^+$  516.1755, found 516.1754.

**Compound 12n:** Yellow solid; Yield: 94%; HPLC purity: 94.55%;  $^1H$ -NMR (600 MHz, DMSO- $d_6$ ):  $\delta$  11.93 (s, 1H), 11.73 (s, 1H), 9.64 (s, 1H), 9.38 (s, 1H), 8.75 (d,  $J=5.1$  Hz, 1H), 8.59 (d,  $J=5.1$  Hz, 1H), 8.55–8.51 (m, 1H), 8.42 (s, 1H), 8.24 (brs, 1H), 7.61 (dd,  $J=5.1$ , 8.1 Hz, 1H), 7.54 (d,  $J=8.1$  Hz, 1H), 7.49–7.39 (m, 2H), 7.32 (s, 1H), 6.92 (s, 2H), 6.63–6.53 (m, 1H), 3.82 (s, 6H);  $^{13}C$ -NMR (150 MHz, DMSO- $d_6$ ):  $\delta$  161.9 (C=O), 148.5 (–CH=N), 55.8 (CH<sub>3</sub>O), aromatic carbon atoms (23C) gave signals at 161.2, 161.0, 159.9, 158.3, 158.1, 151.7, 148.5, 147.4, 136.9, 134.9, 133.7, 132.9, 130.8, 127.4, 124.4, 119.7, 112.7, 111.6, 107.9, 105.3, 104.1, 102.7; ESI-HRMS (+):  $m/z$  calcd for  $C_{27}H_{24}N_7O_3^+$   $[M+H]^+$  494.1935, found 494.1937; calcd for  $C_{27}H_{23}N_7O_3Na^+$   $[M+Na]^+$  516.1755, found 516.1758.

**Compound 12o:** Yellow solid; Yield: 89%; HPLC purity: 92.54%;  $^1H$ -NMR (600 MHz, DMSO- $d_6$ ):  $\delta$  11.89 (s, 1H), 11.73 (s, 1H), 9.63 (s, 1H), 9.37 (s, 1H), 8.74 (d,  $J=5.1$  Hz, 1H), 8.58 (d,  $J=5.1$  Hz, 1H), 8.50 (d,  $J=8.1$  Hz, 1H), 8.42 (s, 1H), 8.24 (s, 1H), 7.58 (dd,  $J=5.1$ , 8.1 Hz, 1H), 7.55 (d,  $J=8.1$  Hz, 1H), 7.47–7.41 (m, 2H), 7.32 (s, 1H), 7.06 (s, 2H), 3.86 (s, 6H), 3.73 (s, 3H);  $^{13}C$ -NMR (150 MHz, DMSO- $d_6$ ):  $\delta$  161.9 (C=O), 148.6 (–CH=N), 60.6 (CH<sub>3</sub>O), 56.4 (CH<sub>3</sub>O), aromatic carbon atoms (23C) gave signals at 161.1, 159.8, 158.1, 153.7, 151.9, 148.1, 147.6, 139.6, 134.8, 133.7, 132.9, 130.8, 130.4, 127.4, 124.4, 119.6, 112.7, 111.6, 107.9, 104.7, 104.0; ESI-HRMS (+):  $m/z$  calcd for  $C_{28}H_{26}N_7O_4^+$   $[M+H]^+$  524.2041, found 524.2040; calcd for  $C_{28}H_{25}N_7O_4Na^+$   $[M+Na]^+$  546.186, found 546.1860.

**Compound 12p:** Yellow solid; Yield: 84%; HPLC purity: 94.34%;  $^1H$  NMR (600 MHz, DMSO- $d_6$ ):  $\delta$  11.86 (s, 1H), 11.75 (s, 1H), 9.64 (s, 1H), 9.39 (s, 1H), 8.76 (s, 1H), 8.71 (brs, 1H), 8.59 (d,  $J=5.1$  Hz, 1H), 8.51 (d,  $J=8.1$  Hz, 1H), 8.25 (s, 1H), 7.70 (d,  $J=5.1$  Hz, 1H), 7.60 (dd,  $J=5.1$ , 8.1 Hz, 1H), 7.56 (d,  $J=8.1$  Hz, 1H), 7.51 (d,  $J=5.1$  Hz, 1H), 7.48–7.42 (m, 2H), 7.29 (s, 1H), 7.18 (t,  $J=5.1$  Hz, 1H);  $^{13}C$  NMR (150 MHz, DMSO- $d_6$ ):  $\delta$  161.9 (C=O), 148.6 (–CH=N), aromatic carbon atoms (21C) gave signals at 161.1, 159.8, 158.0, 151.8, 148.1, 142.6, 139.7, 134.8, 133.7, 132.9, 131.3, 130.8, 129.3, 128.4, 127.4, 124.4, 119.7, 112.7, 111.6, 107.9, 103.9; ESI-HRMS (+):  $m/z$  calcd for  $C_{23}H_{18}N_7OS^+$   $[M+H]^+$  440.1288, found 440.1286; calcd for  $C_{23}H_{17}N_7OSNa^+$   $[M+Na]^+$  462.1107, found 462.1103.

**Compound 12q:** Yellow solid; Yield: 83%; HPLC purity: 97.10%;  $^1H$  NMR (600 MHz, DMSO- $d_6$ ):  $\delta$  11.86 (s, 1H), 11.78 (s, 1H), 9.70 (s, 1H), 9.42 (s, 1H), 8.84 (d,  $J=5.1$  Hz, 1H), 8.71 (d,  $J=8.1$  Hz, 1H), 8.62 (d,  $J=5.1$  Hz, 1H), 8.37 (s, 1H), 8.18 (s, 1H), 7.88 (s, 1H), 7.81–7.75 (m, 1H), 7.55 (d,  $J=8.1$  Hz, 1H), 7.49 (d,  $J=5.1$  Hz, 1H), 7.44 (d,  $J=8.1$  Hz, 1H), 7.27 (s, 1H), 6.97 (s, 1H), 6.67 (s, 1H);  $^{13}C$  NMR (150 MHz, DMSO- $d_6$ ):  $\delta$  161.2 (C=O), 149.1 (–CH=N), aromatic carbon atoms (21C) gave signals at 160.9, 159.9, 159.0, 158.7, 150.0, 149.8, 146.7, 145.6, 137.2, 133.9, 133.7, 133.5, 130.8, 127.4, 125.3, 119.8, 117.0, 113.9, 112.7, 112.0, 108.0, 103.9; ESI-HRMS (+):  $m/z$  calcd for  $C_{23}H_{18}N_7O^+$   $[M+H]^+$  424.1516, found 424.1510; calcd for  $C_{23}H_{17}N_7O_2Na^+$   $[M+Na]^+$  446.1336, found 446.1331.

**Compound 12r:** Yellow solid; Yield: 86%; HPLC purity: 94.56%;  $^1H$  NMR (600 MHz, DMSO- $d_6$ ):  $\delta$  11.98 (s, 1H), 11.71 (s, 1H), 9.67 (s, 1H), 9.44 (d,  $J=8.1$  Hz, 1H), 9.41 (s, 1H), 9.20 (s, 1H), 8.78 (d,  $J=5.1$  Hz, 1H), 8.61 (d,  $J=5.1$  Hz, 1H), 8.57 (d,  $J=8.1$  Hz, 1H), 8.26 (s, 1H), 8.07 (d,  $J=8.1$  Hz, 1H), 7.93 (d,  $J=8.1$  Hz, 1H), 7.64 (dd,  $J=5.1$ , 8.1 Hz, 2H), 7.59–7.52 (m, 2H), 7.48 (d,  $J=8.1$  Hz, 1H), 7.46 (d,  $J=5.1$  Hz, 1H), 7.41 (s, 1H), 4.05 (s, 3H);  $^{13}C$ -NMR (150 MHz, DMSO- $d_6$ ):  $\delta$  161.1 (C=O), 148.4 (–CH=N), 56.4 (CH<sub>3</sub>O), aromatic carbon atoms (25C) gave signals at 160.9, 159.9, 159.1, 157.9, 157.1, 147.9, 146.6, 137.3, 133.8, 133.5, 131.6, 131.1, 129.9, 128.3, 127.5, 126.2, 125.5, 125.4, 124.9, 119.7, 112.7, 112.0, 108.0, 104.9, 103.8; ESI-HRMS (+):  $m/z$  calcd for  $C_{30}H_{24}N_7O_2^+$   $[M+H]^+$

514.1986, found 514.1981; calcd for  $C_{30}H_{23}N_7O_2Na^+$   $[M+Na]^+$  536.1805, found 536.1800.

#### 4.1.7. General procedure for the synthesis of compounds 12A–12F (series C)

Different methyl ketones (1.1 mmol) were separately added to a solution of **11** (1 mmol, 0.345 g) in ethyl 6 ml of alcohol. These mixtures were heated at 78 °C for 10 h, and the solvent was removed from the reaction mixtures under a vacuum. The resulting crude products were purified by flash chromatography on silica gel, eluting with the appropriate mixtures of CH<sub>2</sub>Cl<sub>2</sub> and MeOH to obtain the corresponding compounds **12A–12F** (Series C). Their structures were characterised by NMR and ESI-HRMS. Structures and IUPAC names of these target compounds (Series B) are listed in Table S3 (Supporting Information).

**Compound 12A:** Yellow solid; Yield: 91%; HPLC purity: 93.25%;  $^1H$ -NMR (600 MHz, DMSO- $d_6$ ):  $\delta$  11.71 (s, 1H), 9.65 (s, 1H), 9.39 (brs, 1H), 8.78 (s, 1H), 8.59–8.58 (m, 2H), 8.20 (s, 1H), 7.88 (d,  $J=8.1$  Hz, 2H), 7.70–7.63 (m, 1H), 7.56 (d,  $J=8.1$  Hz, 1H), 7.51–7.43 (m, 6H), 7.42–7.35 (m, 1H), 2.43 (s, 3H);  $^{13}C$ -NMR (150 MHz, DMSO- $d_6$ ):  $\delta$  161.7 (C=O), 147.9 (–CCH<sub>3</sub>=N), 19.0 (CH<sub>3</sub>), aromatic carbon atoms (23C) gave signals at 161.0, 159.8, 151.0, 147.9, 135.7, 133.9, 133.9, 133.6, 133.2, 129.9, 128.9, 127.5, 127.3, 126.9, 124.7, 120.3, 112.7, 111.8, 108.0, 105.2; ESI-HRMS (+):  $m/z$  calcd for  $C_{26}H_{22}N_7O^+$   $[M+H]^+$  448.1880, found 448.1878,  $C_{26}H_{21}N_7O Na^+$   $[M+Na]^+$  470.17, found 470.1698.

**Compound 12B:** Yellow solid; Yield: 88%; HPLC purity: 96.25%;  $^1H$ -NMR (600 MHz, DMSO- $d_6$ ):  $\delta$  11.71 (s, 1H), 10.71 (s, 1H), 9.63 (s, 1H), 9.38 (s, 1H), 8.75 (s, 1H), 8.59 (d,  $J=5.1$  Hz, 1H), 8.51 (d,  $J=8.1$  Hz, 1H), 8.25 (s, 1H), 7.91 (d,  $J=8.1$  Hz, 2H), 7.59 (s, 2H), 7.55 (s, 2H), 7.44 (d,  $J=5.1$  Hz, 2H), 7.40 (s, 1H), 2.42 (s, 3H);  $^{13}C$ -NMR (150 MHz, DMSO- $d_6$ ):  $\delta$  164.9 (C=O), 148.6 (–CCH<sub>3</sub>=N), 19.0 (CH<sub>3</sub>), aromatic carbon atoms (23C) gave signals at 161.9, 161.1, 159.8, 153.3, 151.8, 137.5, 134.8, 134.5, 133.7, 132.9, 129.7, 129.0, 128.6, 127.5, 124.4, 121.1, 119.7, 112.7, 111.7, 109.5, 107.9; ESI-HRMS (+):  $m/z$  calcd for  $C_{26}H_{21}ClN_7O^+$   $[M+H]^+$  482.1491, found 482.1491,  $C_{26}H_{20}ClN_7ONa^+$   $[M+Na]^+$  504.1310, found 504.1311.

**Compound 12C:** Yellow solid; Yield: 91%; HPLC purity: 94.05%;  $^1H$ -NMR (600 MHz, DMSO- $d_6$ ):  $\delta$  11.77 (s, 1H), 9.70 (s, 1H), 9.43 (d,  $J=2.0$  Hz, 1H), 8.83 (dd,  $J=2.0$ , 5.1 Hz, 1H), 8.69 (td,  $J=2.0$ , 8.1 Hz, 1H), 8.62 (d,  $J=5.1$  Hz, 1H), 8.34 (d,  $J=8.1$  Hz, 2H), 8.23 (s, 1H), 8.13 (d,  $J=8.1$  Hz, 2H), 7.76 (dd,  $J=5.1$ , 8.1 Hz, 1H), 7.57 (d,  $J=8.1$  Hz, 1H), 7.49 (d,  $J=5.1$  Hz, 1H), 7.46 (d,  $J=8.1$  Hz, 1H), 7.44 (d,  $J=2.0$  Hz, 1H), 2.49 (s, 3H);  $^{13}C$ -NMR (150 MHz, DMSO- $d_6$ ):  $\delta$  161.1 (C=O), 148.0 (–CCH<sub>3</sub>=N), 27.5 (CH<sub>3</sub>), aromatic carbon atoms (23C) gave signals at 160.8, 159.9, 149.5, 146.4, 144.8, 141.7, 137.4, 133.7, 133.4, 130.0, 128.2, 127.9, 127.5, 125.4, 124.2, 124.1, 120.1, 112.9, 112.8, 112.1, 108.0; ESI-HRMS (+):  $m/z$  calcd for  $C_{26}H_{21}N_8O_3^+$   $[M+H]^+$  493.1731, found 493.1732,  $C_{26}H_{20}N_8O_3Na^+$   $[M+Na]^+$  515.1551, found 515.1552.

**Compound 12D:** Yellow solid; Yield: 87%; HPLC purity: 94.55%;  $^1H$  NMR (DMSO- $d_6$ ):  $\delta$  11.69 (s, 1H), 9.62 (s, 1H), 9.37 (s, 1H), 8.75 (d,  $J=5.1$  Hz, 1H), 8.58 (d,  $J=5.1$  Hz, 1H), 8.51 (d,  $J=8.1$  Hz, 1H), 8.22 (s, 1H), 7.78 (d,  $J=8.1$  Hz, 2H), 7.62–7.52 (m, 2H), 7.48–7.42 (m, 2H), 7.39 (s, 1H), 7.29 (s, 1H), 2.40 (s, 3H), 2.37 (s, 3H);  $^{13}C$  NMR (150 MHz, DMSO- $d_6$ ):  $\delta$  161.9 (C=O), 148.5 (–CCH<sub>3</sub>=N), 40.3 (CH<sub>3</sub>), 21.3 (CH<sub>3</sub>), aromatic carbon atoms (23C) gave signals at 161.0, 159.8, 156.3, 151.8, 139.6, 135.8, 134.9, 133.6, 132.9, 129.7, 129.5, 128.7, 127.5, 126.8, 124.5, 119.6, 112.7, 111.8, 108.0, 104.7, 102.6; ESI-HRMS (+):  $m/z$  calcd for  $C_{27}H_{24}N_7O^+$   $[M+H]^+$  462.2037, found 462.2035,  $C_{27}H_{23}N_7O^+$   $[M+Na]^+$  484.1856, found 484.1856.

**Compound 12E:** Yellow solid; Yield: 90%; HPLC purity: 91.25%;  $^1\text{H-NMR}$  (600 MHz,  $\text{DMSO-d}_6$ ):  $\delta$  13.45 (s, 1H), 11.81 (s, 1H), 11.33 (s, 1H), 9.65 (s, 1H), 9.38 (s, 1H), 8.76 (d,  $J=5.0$  Hz, 1H), 8.59 (d,  $J=5.0$  Hz, 1H), 8.54 (td,  $J=2.0$ , 8.1 Hz, 1H), 8.24 (s, 1H), 7.78 (d,  $J=2.0$  Hz, 1H), 7.63 (dd,  $J=5.1$ , 8.1 Hz, 1H), 7.58 (dd,  $J=2.0$ , 8.1 Hz, 1H), 7.49–7.44 (m, 4H), 6.92 (d,  $J=8.1$  Hz, 1H), 2.54 (s, 3H);  $^{13}\text{C-NMR}$  (150 MHz,  $\text{DMSO-d}_6$ ):  $\delta$  161.8 (C=O), 148.3 (– $\text{CCH}_3=\text{N}$ ), 14.7 ( $\text{CH}_3$ ), aromatic carbon atoms (23 C) gave signals at 161.0, 159.8, 159.0, 158.3, 158.0, 151.6, 135.2, 134.0, 133.9, 133.8, 133.0, 131.0, 129.8, 127.4, 124.5, 122.1, 120.0, 120.0, 112.7, 111.7, 110.1, 108.0, 105.8; ESI-HRMS (+):  $m/z$  calcd for  $\text{C}_{26}\text{H}_{21}\text{BrN}_7\text{O}_2^+$  [ $\text{M} + \text{H}$ ] $^+$  542.0935, found 542.0934,  $\text{C}_{26}\text{H}_{20}\text{BrN}_7\text{O}_2\text{Na}^+$  [ $\text{M} + \text{Na}$ ] $^+$  564.0754, found 564.0752.

**Compound 12F:** Yellow solid; Yield: 91%; HPLC purity: 94.67%;  $^1\text{H-NMR}$  (600 MHz,  $\text{DMSO-d}_6$ ):  $\delta$  11.83 (s, 1H), 11.24 (s, 1H), 9.78–9.63 (m, 1H), 9.47–9.23 (m, 1H), 8.82 (s, 1H), 8.67 (d,  $J=8.1$  Hz, 1H), 8.62 (d,  $J=5.1$  Hz, 1H), 8.21 (s, 1H), 7.75 (s, 1H), 7.59 (d,  $J=8.1$  Hz, 1H), 7.51–7.40 (m,  $J=8.1$  Hz, 3H), 7.16 (s, 1H), 6.96 (d,  $J=8.1$  Hz, 1H), 6.88 (d,  $J=8.1$  Hz, 1H), 2.55 (s, 3H);  $^{13}\text{C-NMR}$  (150 MHz,  $\text{DMSO-d}_6$ ):  $\delta$  161.3 (C=O), 147.0 (– $\text{CCH}_3=\text{N}$ ), 56.1 ( $\text{CH}_3\text{O}$ ), 14.7 ( $\text{CH}_3$ ), aromatic carbon atoms (23 C) gave signals at 161.0, 159.9, 159.0, 158.7, 153.0, 151.9, 150.2, 136.7, 134.0, 133.6, 133.6, 130.1, 127.4, 125.1, 120.0, 118.3, 118.0, 117.3, 113.3, 112.7, 111.9, 108.1, 105.6; ESI-HRMS (+):  $m/z$  calcd for  $\text{C}_{27}\text{H}_{24}\text{N}_7\text{O}_3^+$  [ $\text{M} + \text{H}$ ] $^+$  494.1935, found 494.1938,  $\text{C}_{27}\text{H}_{23}\text{N}_7\text{O}_3\text{Na}^+$  [ $\text{M} + \text{Na}$ ] $^+$  516.1755, found 516.1758.

## 4.2. Biologicals

### 4.2.1. Cell lines and cell culture

The HeLa, MDA-MB-231, HepG2, MCF-7, NT2, A549, A375, A875, HeCat, and LO2 cell lines were cultured in complete Dulbecco's modified Eagle's medium (DMEM; Basal Media, D120716) supplemented with 10% foetal bovine serum (900–108; Gemini Bio = Products Inc., Calabasas, CA, USA). The MCF-10A cell line was cultured in Lonza MEGM<sup>TM</sup> Bullet Kit (CC-3151 & CC-4136; Lonza Group AG, Basel, Switzerland) containing 2 mg/mL insulin, 1 mg/mL hydrocortisone, 100 U/mL penicillin, 100  $\mu\text{g}/\text{mL}$  EGF, and 100  $\mu\text{g}/\text{mL}$  streptomycin and 5% horse serum. All cells were incubated in a humidified atmosphere (5%  $\text{CO}_2$ , 95% air) at 37 °C.

### 4.2.2. Cell viability assay

Cancer cells were cultured in DMEM in a 96-well plate and treated with each compound at 0.1, 1, 5, 10, 20, 50  $\mu\text{M}$ , with eight replicates for each concentration. After treatment for 48 h, the cells were subjected to MTT assay with some modifications. Briefly,  $5 \times 10^3$  cells were seeded in each well of a 96-well plate with 100  $\mu\text{L}$  of DMEM. Before treatment, cells were allowed to adhere for 24 h. All the compounds were dissolved in DMSO with a stock solution of 20  $\mu\text{M}$  and subsequent dilutions were made with DMEM medium. Treatment with 0.5% DMSO was used as control. After 48 h treatment, 20  $\mu\text{L}$  of MTT solution (5 mg/mL) was added into each well, followed by incubation for 4 h. Then, the supernatant medium was removed and 100  $\mu\text{L}$  DMSO was added to each well. The absorbance value of each well was recorded at 490 nm on a Multiskan<sup>TM</sup> FC microplate reader (Thermo Fisher Scientific Inc.) and the DMSO treatment group was considered as 100% viability. The  $\text{IC}_{50}$  and error values were calculated using the GraphPad Prism 8 software (GraphPad software Inc., San Diego, CA, USA) using the absorbance values recorded at 490 nm.

### 4.2.3. Western blot analysis

After treatment with the compounds, the cells were boiled with  $1 \times$  SDS loading buffer at 100 °C, for 10 min. The boiled samples were subjected to 8%–12% sodium dodecyl sulfate-polyacrylamide gel electrophoresis (SDS-PAGE), then transferred to polyvinylidene fluoride (PVDF) membrane (03010040001; Hoffmann-La Roche AG, Basel, Switzerland). The proteins were probed with indicated primary antibodies and then secondary antibodies. After incubating with enhanced chemiluminescence (ECL) reagents, the membranes were exposed to films and then films were developed to visualise the immunoreactive protein bands.

### 4.2.4. Quantitative real-time PCR (qRT-PCR) analysis

The qRT-PCR analysis was performed as previously described with some modifications<sup>[30]</sup>. Briefly, cells were harvested and total RNA was extracted. Then, the cDNAs were obtained by reverse transcription using the RevertAid RT Reverse Transcription Kit (K1691; Thermo Fisher Scientific Inc.) following the manufacturer's protocol. Then, qRT-PCR was conducted for the measurement of mRNA expression levels. The following primers were used:

- CHOP sense: 5'-TCTTGACCCTGCTTCTCTG-G-3'.
- Antisense: 5'-GCTGTGCCACTTTCCTTTCA-3'.
- GAPDH sense: 5'-CCAAGGAGTAAGACCCCTGG-3'.
- Antisense: 5'-TGGTTGAGCACAGGGTACTT-3'.

### 4.2.5. Cell apoptosis assay

An Annexin V–fluorescein isothiocyanate (FITC) Apoptosis Detection Kit (BD Biosciences, San Jose, CA, USA) was used to measure cell apoptosis. Cells (about  $1 \times 10^5/\text{well}$ ) cultured in a 6-well plate were treated with **12A** or DMSO for 24 h, and then subjected to apoptosis assay following the kit manufacturer's protocol. After double-staining with FITC annexin V/propidium iodide (PI), the apoptosis status of the cells was detected using the Attune NxT flow cytometer (Thermo Fisher Scientific Inc.) and the data were analysed with the FlowJo 7.6 software (BD Biosciences).

### 4.2.6. In vivo tumor model

We established a mice hepatoma homograft model following a previously reported method<sup>15</sup>. When each tumour grew to about 100  $\text{mm}^3$ , mice were randomly assigned into groups and treated by i.p. injection with the vehicle [1% DMSO + 10% PEG400 (w/v) (Sigma-Aldrich, Saint Louis, MO, USA)] in normal saline or compound **12A** formulated in the vehicle at doses of 20 and 50 mg/kg every other day, respectively. At 6 h after the final dose, mice were euthanized, and tumours were separated, weighed, and subjected to further analysis. All procedures were performed in compliance with the guidelines from the Institutional Animal Care and Use Committee at the Experimental Animal Centre of Xiamen University.

### 4.2.7. Haematoxylin and eosin staining

The staining procedure for H&E followed a previously reported method<sup>15</sup>.

## Acknowledgement

We are grateful to Lijuan Wang, Cuiling Sun, Rong Ding, and Junjie Chen for assistance in the melting point assay, the NMR



experiment, the MS experiment, and the surface plasmon resonance assay, respectively.

## Disclosure statement

No potential conflict of interest was reported by the author(s).

## Funding

The research was supported in part by grants from the Fundamental Research Funds for the Central Universities of China [No. 20720180051], the National Key R&D Program of China [2018YFA0107303], the National Natural Science Foundation of China [No. 81672955], the Fujian Provincial Natural Science Foundation [No. 2018J01132], the Jinhua Science and Technology Plan Project of China [2020-4-088], and the Health Commission of Zhejiang Province of China [2020KY628].

## References

- Wang Y, Xu K, Zhang H, et al. Retinal ganglion cell death is triggered by paraptosis via reactive oxygen species production: a brief literature review presenting a novel hypothesis in glaucoma pathology. *Mol Med Rep* 2014;10:1179–83.
- Maltese WA, Overmeyer JH. Methuosis: nonapoptotic cell death associated with vacuolization of macropinosome and endosome compartments. *Am J Pathol* 2014;184:1630–42.
- Grace NJ, Lopus M. Cell death mechanisms in eukaryotes. *Cell Biol Toxicol* 2020;36:145–64.
- Colin M, Delporte C, Janky R, et al. Dysregulation of macropinocytosis processes in glioblastomas may be exploited to increase intracellular anti-cancer drug levels: the example of temozolomide. *Cancers* 2019;11:411.
- Maltese WA, Overmeyer JH. Non-apoptotic cell death associated with perturbations of macropinocytosis. *Front Physiol* 2015;6:38.
- Cingolani F, Simbari F, Abad JL, et al. Jaspine B induces non-apoptotic cell death in gastric cancer cells independently of its inhibition of ceramide synthase. *J Lipid Res* 2017;58:1500–13.
- Robinson MW, Overmeyer JH, Young AM, et al. Synthesis and evaluation of indole-based chalcones as inducers of methuosis, a novel type of nonapoptotic cell death. *J Med Chem* 2012;55:1940–56.
- Trabbic CJ, Dietsch HM, Alexander EM, et al. Differential induction of cytoplasmic vacuolization and methuosis by novel 2-indolyl-substituted pyridinylpropenones. *ACS Med Chem Lett* 2014;5:73–7.
- Gong X, Sun R, Gao Z, et al. Tubeimoside 1 acts as a chemotherapeutic synergist via stimulating macropinocytosis. *Front Pharmacol* 2018;9:1044.
- Huang W, Sun X, Li Y, et al. Discovery and identification of small molecules as methuosis inducers with *in vivo* antitumor activities. *J Med Chem* 2018;61:5424–34.
- Overmeyer JH, Young AM, Bhanot H, Maltese WA. A chalcone-related small molecule that induces methuosis, a novel form of non-apoptotic cell death, in glioblastoma cells. *Mol Cancer* 2011;10:69.
- Pang L, Liu CY, Gong GH, Quan ZS. Synthesis, *in vitro* and *in vivo* biological evaluation of novel lappaconitine derivatives as potential anti-inflammatory agents. *Acta Pharm Sin B* 2020;10:628–45.
- Trabbic CJ, George SM, Alexander EM, et al. Synthesis and biological evaluation of isomeric methoxy substitutions on anti-cancer indolyl-pyridinyl-propenones: effects on potency and mode of activity. *Eur J Med Chem* 2016;122:79–91.
- Lertsuwan J, Lertsuwan K, Sawasdichai A, et al. CX-4945 induces methuosis in cholangiocarcinoma cell lines by a CK2-independent mechanism. *Cancers* 2018;10:283.
- Qin J, Liu J, Wu C, et al. Synthesis and biological evaluation of (3/4-(pyrimidin-2-ylamino)benzoyl)-based hydrazine-1-carboxamide/carbothioamide derivatives as novel RXR $\alpha$  antagonists. *J Enzyme Inhib Med Chem* 2020;35:880–96.
- Hu H, Wu J, Ao M, et al. Design, synthesis and biological evaluation of methylenehydrazine-1-carboxamide derivatives with (5-((4-(pyridin-3-yl)pyrimidin-2-yl)amino)-1H-indole scaffold: Novel potential CDK9 inhibitors. *Bioorg Chem* 2020;102:104064.
- Cortes-García CJ, Islas-Jácome A, Rentería-Gómez A, et al. Synthesis of 1,5-disubstituted tetrazoles containing a fragment of the anticancer drug imatinib via a microwave-assisted Ugi-azide reaction. *Monatshefte für Chemie – Chem Monthly* 2016;147:1277–90.
- Li YT, Wang JH, Pan CW, et al. Syntheses and biological evaluation of 1,2,3-triazole and 1,3,4-oxadiazole derivatives of imatinib. *Bioorg Med Chem Lett* 2016;26:1419–27.
- Buclin T, Thoma Y, Widmer N, et al. The steps to therapeutic drug monitoring: a structured approach illustrated with imatinib. *Front Pharmacol* 2020;11:177.
- Hu H, Wu J, Ao M, et al. Synthesis, structure-activity relationship studies and biological evaluation of novel 2,5-disubstituted indole derivatives as anticancer agents. *Chem Biol Drug Des* 2016;88:766–78.
- Busschaert N, Kirby IL, Young S, et al. Squaramides as potent transmembrane anion transporters. *Angew Chem Int Ed Engl* 2012;51:4426–30.
- Morales S, Aceña JL, García Ruano JL, Cid MB. Sustainable synthesis of oximes, hydrazones, and thiosemicarbazones under mild organocatalyzed reaction conditions. *J Org Chem* 2016;81:10016–22.
- Pan X, Wang F, Zhang Y, et al. Design, synthesis and biological activities of Nilotinib derivatives as antitumor agents. *Bioorganic Med Chem* 2013;21:2527–34.
- Sperandio S, de Belle I, Bredesen DE. An alternative, nonapoptotic form of programmed cell death. *Proc Natl Acad Sci USA* 2000;97:14376–81.
- Kim SH, Kang JG, Kim CS, et al. The hsp70 inhibitor VER155008 induces paraptosis requiring de novo protein synthesis in anaplastic thyroid carcinoma cells. *Biochem Biophys Res Commun* 2014;454:36–41.
- Sperandio S, Poksay K, de Belle I, et al. Paraptosis: mediation by MAP kinases and inhibition by AIP-1/Alix. *Cell Death Different* 2004;11:1066–75.
- Li Z, Mbah NE, Overmeyer JH, et al. The JNK signaling pathway plays a key role in methuosis (non-apoptotic cell death) induced by MOMIPP in glioblastoma. *BMC Cancer* 2019;19:77.
- Li X, Yang J, Peng L, et al. Triple-negative breast cancer has worse overall survival and cause-specific survival than non-triple-negative breast cancer. *Breast Cancer Res Treat* 2017;161:279–87.

29. Hwang SY, Park S, Kwon Y. Recent therapeutic trends and promising targets in triple negative breast cancer. *Pharmacol Ther* 2019;199:30–57.
30. Wu J, Xue YH, Gao X, Zhou Q. Host cell factors stimulate HIV-1 transcription by antagonizing substrate-binding function of Siah1 ubiquitin ligase to stabilize transcription elongation factor ELL2. *Nucleic Acids Research* 2020;48:7321–32.